*applied system innovation*

MDPI

*Article*

# Seismic and Structural Analyses of the Eastern Anatolian Region (Turkey) Using Different Probabilities of Exceedance

**Ercan Işık [1], Ehsan Harirchian [2,*], Aydın Büyüksaraç [3] and Yunus Levent Ekinci [4]**

[1] Department of Civil Engineering, Bitlis Eren University, Bitlis 13100, Turkey; eisik@beu.edu.tr
[2] Institute of Structural Mechanics (ISM), Bauhaus-Universität Weimar, 99423 Weimar, Germany
[3] Çan Vocational School, Çanakkale Onsekiz Mart University, Çanakkale 17400, Turkey; absarac@comu.edu.tr
[4] Department of Art History, Bitlis Eren University, Bitlis 13100, Turkey; ylekinci@beu.edu.tr
* Correspondence: ehsan.harirchian@uni-weimar.de

**Abstract:** Seismic hazard analysis of the earthquake-prone Eastern Anatolian Region (Turkey) has become more important due to its growing strategic importance as a global energy corridor. Most of the cities in that region have experienced the loss of life and property due to significant earthquakes. Thus, in this study, we attempted to estimate the seismic hazard in that region. Seismic moment variations were obtained using different types of earthquake magnitudes such as Mw, Ms, and Mb. The earthquake parameters were also determined for all provincial centers using the earthquake ground motion levels with some probabilities of exceedance. The spectral acceleration coefficients were compared based on the current and previous seismic design codes of the country. Additionally, structural analyses were performed using different earthquake ground motion levels for the Bingöl province, which has the highest peak ground acceleration values for a sample reinforced concrete building. The highest seismic moment variations were found between the Van and Hakkari provinces. The findings also showed that the peak ground acceleration values varied between 0.2–0.7 g for earthquakes, with a repetition period of 475 years. A comparison of the probabilistic seismic hazard curves of the Bingöl province with the well-known attenuation relationships showed that the current seismic design code indicates a higher earthquake risk than most of the others.

**Keywords:** Eastern Turkey; site-specific spectra; seismic hazard; seismic moment



**Citation:** Işık, E.; Harirchian, E.; Büyüksaraç, A.; Levent Ekinci, Y. Seismic and Structural Analyses of the Eastern Anatolian Region (Turkey) Using Different Probabilities of Exceedance. *Appl. Syst. Innov.* **2021**, *4*, 89. https://doi.org/10.3390/asi4040089

Academic Editor: Andrey Chernov

Received: 28 September 2021
Accepted: 6 November 2021
Published: 11 November 2021



## 1. Introduction

Earthquake risk is defined as the probability of ground motion that can damage and cause loss of life in a certain place within a certain time period. Seismic hazard analysis is an essential stage for the estimation of earthquake risk. Earthquake parameters such as the peak ground acceleration (PGA), peak ground velocity (PGV), and spectral acceleration may be obtained by traditional probabilistic seismic hazard analyses. Mostly, these parameters are obtained using the annual probability of exceedance for a specific location of the event and design characteristics [1–6]. Significant loss of life and property after an earthquake's occurrence clearly shows the importance of the seismic hazard estimation studies. Assessing and managing the necessary information about earthquakes are also important factors for spatial planning and urban renewal [7–12]. The seismic design codes and earthquake hazard maps can be updated through the new data obtained. In this way, potential seismic hazard estimations can be made more realistically.

The studies of reducing earthquake damage started after the Erzincan earthquake (Mw = 7.9), which was recorded as the biggest earthquake in Turkey; 33,000 people lost their lives. Turkey's first seismic zoning map was officially produced in 1945 [13,14]. This map was updated in 1945, 1947, 1963, 1972, 1996, and 2019. Except for the latest map, the previous ones were produced based on regional risk. The last updated map was produced by taking into account earthquake hazards based on specific sites. The current map was

prepared within the scope of a project titled "Updating the Seismic Hazard Map of Turkey", which was supported by the Disaster and Emergency Management Presidency of Turkey (DEMP) in the scope of the National Earthquake Research Program (UDAP). The latest updated map was prepared in a more detailed manner using the recent earthquake source parameters, earthquake catalogues, and also the newest mathematical models. Dissimilar to the previous ones, PGA values are starting to be used, and the approach of "earthquake risk regions" lost its significance [14–17]. In the updated Turkish Earthquake Hazard Map, both the horizontal and vertical spectral parameters can be obtained for four earthquake ground motion levels, which are given in the following sections. In this map, seismic risk is defined probabilistically due to its uncertainties related to geographical location [18]. Technological developments and scientific innovations in civil and earthquake engineering have necessitated some changes in earthquake-resistant building design principles. So far, 10 different seismic design codes have come into force at different times in Turkey. The most detailed and up-to-date one was completed in 2018 and entered into use in 2019. In this study, the effects of different earthquake ground motion levels and site-specific design spectrums on structural analyses were examined on a regional basis. In the previous code, only the standard design earthquake motion with a repetition period of 475 years was in question. However, 4 different ground motion levels with 2475, 475, 72, and 43 repetition periods are taken into account with the current regulation. Another innovation taken into account in this study is the site-specific design spectra. In the previous code, four different design spectra were being used for a total of four different earthquake zones. A design spectrum specific to each geographical location is used with the current map and code.

Seismic forces threating the structures are directly related to the ground motions. One of the most important terms for determining these forces are the design spectra. There is a need to update the earthquake hazard map, providing input data to the design spectra obtained from seismic zoning. Hence, seismic zoning studies for ground motions are important indicators in determining seismic risk. In this context, the effects of ground motion on structures and the target displacements expected from the structure can be obtained more realistically using microzoning and site-specific analyses of seismic hazards. In microzoning studies, the region is divided into subregions, and efficient plans and strategies can be performed to minimize earthquake damages. Thus, using technological developments, economical potential, and scientific approaches, seismic microzoning has started to be used in the country with the updated Turkish Earthquake Hazard Map. Henceforth, site-specific seismic hazard analyses for any geographic location can be performed by using this map.

In this study, the seismic risk of the Eastern Anatolian Region was evaluated using a performance-based earthquake engineering approach. This approach aims at improving seismic risk decision making through assessment and design methods that have a strong scientific background and express options that enable stakeholders to make informed decisions. It includes four processing steps such as hazard analysis, structural or nonstructural analyses, and damage and loss estimations. The first step requires hazard analysis, in which one or more ground motion Intensity Measurements (IMs) are evaluated. The IM is obtained independently from local soil conditions by conventional probabilistic seismic hazard analysis for a standard earthquake. Generally, an IM is defined by an associated average annual probability of exceedance, which is specific to the location and design characteristics of the region [4,19,20]. It is possible to quantify the damage levels that may occur under the design's ground motion within the structural system elements in the performance-based design and evaluation method. Acceptable damage limits are defined to be consistent with the expected performance targets at various earthquake ground motion levels [21,22]. First, the earthquake demand is calculated in performance-based design and assessment methods. It is then necessary to determine the structural performance by comparing these demand values with the deformation capacity for the selected performance levels [23–26]. However, it may not reflect the expected state of the design, since the acceleration values given in the standards cannot clearly meet the actual physical conditions in which the buildings exist [27–30]. According to the Turkish

Earthquake Building Code (TBEC-2018) [31], the demand spectra are determined for the seismic performance of an existing building based on a different probability of exceedance in 50 years.

The Eastern Anatolia Region is seismically very active region. The 2003 Bingöl (Mw = 6.4), 2011 Van (Mw = 7.2), and 2020 Elazığ (Mw = 6.8) earthquakes reveal the seismic hazard in the region. Earthquake-prone regions may be determined—and significant contributions can be made—to update seismic design codes by using the data obtained from destructive earthquakes. In this context, the effects of the 2011 Van earthquakes in particular contributed to the development of the the TBEC-2018 [31]. Moreover, it is mandatory to use an earthquake hazard map with this updated code. The earthquake building parameters can be obtained for any location through this map [31,32]. Here, all provincial centers in the Eastern Anatolia Region (Figure 1) were studied. The seismic moment (Mo) variations for the region were obtained using different types of earthquake magnitudes such as Mw, Ms, and Mb. Additionally, using the earthquake ground motion levels with 2%, 10%, 50%, and 68% probability of exceedance within a 50-year period, the short-period map spectral acceleration coefficient ($S_s$), map spectral acceleration coefficient for 1 s ($S_1$), PGA, and PGV were calculated. The earthquake ground motion level (DD-2) was used to obtain the horizontal and vertical elastic design spectra for all provinces. Aside from that, these spectra were compared for the Bingöl province, which has the highest PGA. The spectra obtained for this province were compared with different seismic attenuation relationships.


**Figure 1.** The location map showing the provincial centers in the Eastern Anatolian Region.

There are some studies about the differences between previous and updated earthquake codes and maps. In those studies, the seismic force calculation methods, base shear forces, displacements, period, target displacements, spectra, local soil conditions, and section damage values were examined [33–44]. In those studies, changes in the seismicity parameters on a provincial or regional basis or changes in the structural analyses on a sample structure were examined. In this study, both the earthquake and structural analysis results were obtained for all provinces in the region, and the results were compared. Here, the Eastern Anatolian Region, which has the longest active fault length in Turkey and is highly active in terms of seismicity, was chosen as an example, and all the provinces in the region were taken into account. The investigation of the effect of different earthquake ground motion levels on building earthquake behavior makes this study different from the other studies. The spectral responses for different exceedance of probabilities for the Bingöl province, which has the highest PGA in the region, were compared with different

attenuation relationships. Additionally, distribution of seismic moments in Eastern Anatolia was carried out according to the current earthquake data. Based on these current data, an image map was produced to obtain the seismic moment distribution in the region.

## 2. Materials and Methods

*Seismicity of the Eastern Anatolia Region*

The region is located where the Arabian and African Plates move toward the Eurasian Plate. This compressional regime controls the formation of many active faults and the seismicity of the region. The general tectonic structure of the region is mainly controlled by the deformation zone known as the Bitlis Zagros Thrust Fault Belt (BZTFB), where the northward-moving Arabian Plate collides with the Anatolian Plate. The dominant fault zones in the region are the East Anatolian Fault Zone (EAFZ), the North Anatolian Fault Zone (NAFZ), and the BZTFB. The collision is managed through the Karlıova Triple Junction, where the right lateral strike-slip NAFZ joins with the left lateral EAFZ (Figure 2). Additionally, to the east of this junction, the dominant elements are mostly NW-SE striking right-lateral and NE-SW striking left-lateral faults. The E-W striking Muş, Lake Van, and Pasinler ramp basins are the other significant tectonic elements in the Eastern Anatolian Region. Due to this active tectonic regime mentioned above, the region has experienced numerous earthquakes so far. The distributions of the historical and recent earthquakes (Ms $\geq$ 3.0) produced from the database of the DEMP for the country are given in Figure 3.

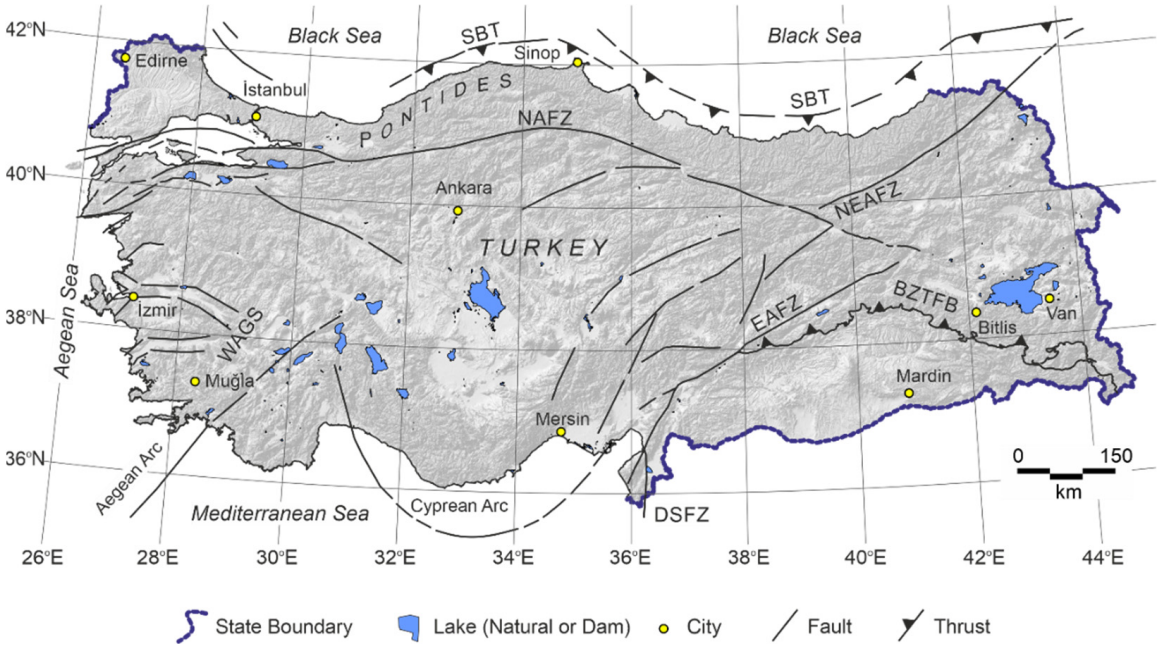


**Figure 2.** Simplified neotectonic and relief maps of Turkey and the surrounding area [45–49]. SBT: Southern Black Sea Thrust; NAFZ: North Anatolian Fault Zone; NEAFZ: Northeast Anatolian Fault Zone; WAEP: West Anatolia Extensional Province; EAFZ: East Anatolian Fault Zone; DSFZ: Dead Sea Fault Zone; BZTFB: Bitlis Zagros Thrust Fault Belt.

After the collision of the Eurasian and Arabian Plates, Eastern Anatolia has contracted an average of 40–60% in the N-S direction in the last 10 million years (which began in the Middle Miocene in the neotectonic period), and the Earth's crust has thickened and increased in the region [50]. The NAFZ and the EAFZ limit the Eastern Anatolia Region in the west. As a result of the compression in the region, generally, E-W striking, N- or S-dipping high-angle thrusts, folds with E-W striking axes, left-lateral strike-slip faults with NE-SW striking, right-lateral strike-slip faults with NW-SE striking, and N-S striking extensional fractures and volcanic activity related to these fractures were formed. In the region and to the north in the Caucasus, the N-S compression movement was found to be 30 mm/year, and it was stated that 10–40% of the deformation here was related to

earthquakes. A significant part of the deformation passes over the EAFZ, which forms the border of this region with the Anatolian Plate in the west. In the region, inter-mountain depression basins have formed lateral slip faults, opening cracks, folded-thrust areas, and Plio-Quaternary (2 my) volcanic eruptions by jamming [51].

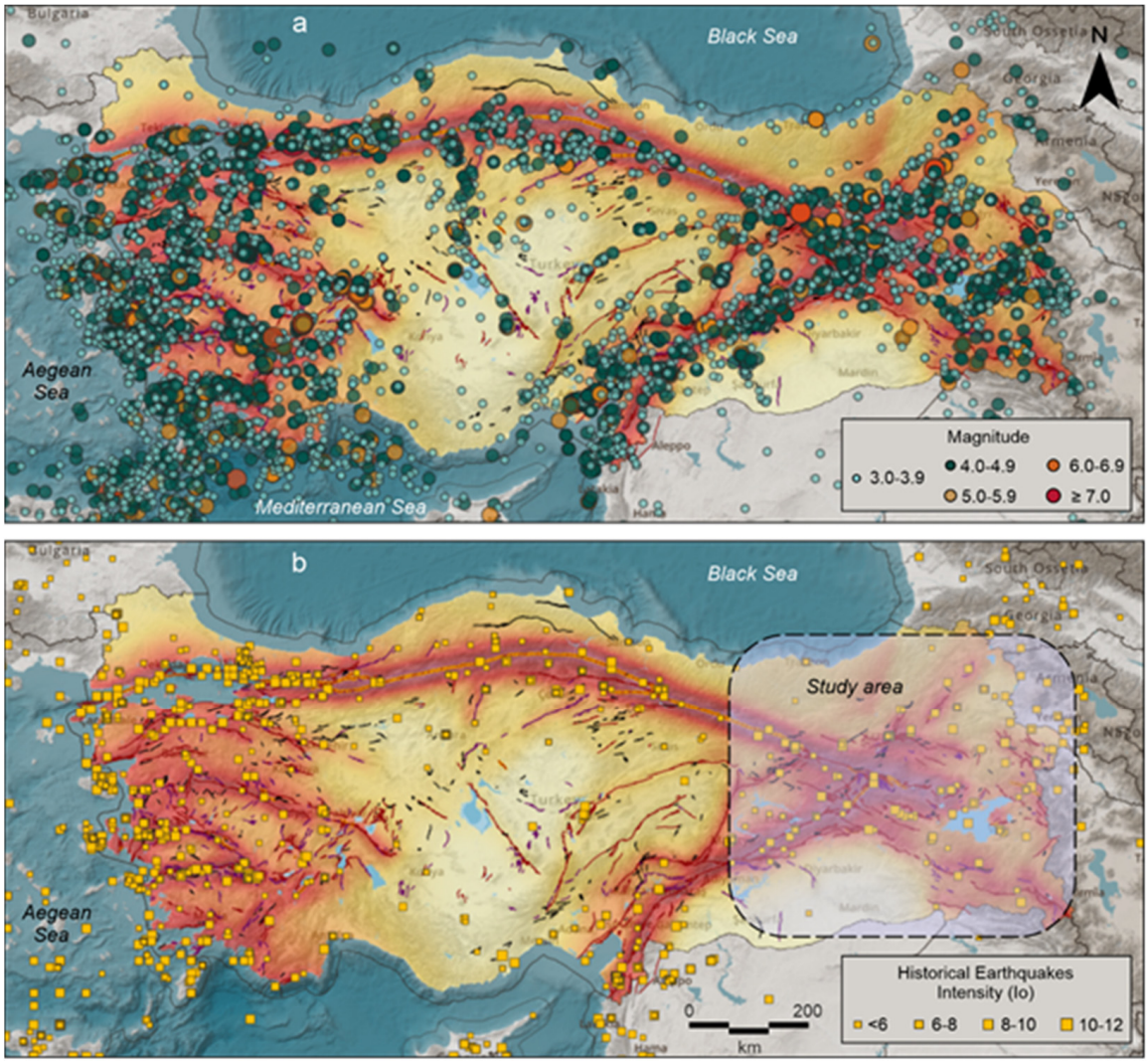


**Figure 3.** Historical and recent seismicity in Eastern Anatolia. (**a**) Distribution of earthquakes (Ms ≥ 3.0) for the instrumental period (1900 < M < 2020). (**b**) Distribution of intensity (Io) according to the MMI scale. Two maps were produced using the database of the DEMP.

Most of the earthquakes in the region occurred at depths of 2–10 km. Except for the EAFZ, one of the main active faults in the region is the Narman-Horasan Fault, which is a left-sided strike-slip fault [52]. The northern part of this fault produced the Narman earthquake (1983). The Çaldıran Fault is a right-sided strike-slip, and it produced the Çaldıran earthquake (1976). An average surface rupture of 50 km was observed. The Tendürek-Balıkgöl Fault contains normal faults in the Balıkgölü section and becomes a distinctly right-sided strike-slip fault toward the southeast of the lake. It was stated that the 1840 Ağrı earthquake was related to this fault [53]. The Karayazı Fault is located parallel to the Tutak Fault at a distance of 15–20 km. Both faults are right-handed and strike-slip [54]. The Erzurum-Tortum Fault has left-sided strike-slip characteristics. The width of the area covered by shear cracks along the belt is up to 10 km. The southern part of this fault produced some earthquakes that caused significant losses in the vicinity of Erzurum province in 1200, 1482, and 1859 [53]. Some of the historical earthquakes that

occurred between the years 240 and 1893 are shown in Table 1 [55–59]. The strongest earthquake occurred in the Çaldıran-Bitlis region with an intensity of X, which corresponds to a magnitude of >7. It is seen that such strong earthquakes were occurring in the vicinity of the Erzincan province.

**Table 1.** Significant historical earthquakes in the Eastern Anatolian Region. The Modified Mercalli Intensity Scale was used as the intensity scale (between I (min) and XII (max)).

| No | Date | Region | Intensity (MMI) (Io) | No | Date | Region | Intensity (MMI) (Io) | No | Date | Region | Intensity (MMI) (Io) |
|---|---|---|---|---|---|---|---|---|---|---|---|
| 1 | 240 | Kayseri-Malatya | IX | 13 | 1374 | Erzincan | VIII | 25 | 1790 | Erzurum | VIII |
| 2 | 771 | Fırat Basin | VIII | 14 | 1422 | Erzincan | VIII | 26 | 1852 | Erzurum | IX |
| 3 | 802 | Fırat Basin | VIII | 15 | 1441 | Van-Bitlis | VIII | 27 | 1859 | Erzurum | IX |
| 4 | 995 | Palu-Sivrice | VI | 16 | 1458 | Erzincan | IX | 28 | 1866 | Erzurum | VIII |
| 5 | 1011 | Erzurum | VIII | 17 | 1482 | Erzincan | IX | 29 | 1868 | Erzurum | IX |
| 6 | 1045 | Erzincan | IX | 18 | 1584 | Erzincan | IX | 30 | 1871 | Ağrı | VIII |
| 7 | 1111 | Van-Ahlat | IX | 19 | 1647 | Van-Bitlis | IX | 31 | 1874 | Elazığ | IX |
| 8 | 1245 | Ahlat-Van | VIII | 20 | 1696 | Çaldıran-Bitlis | X | 32 | 1875 | Erzurum | IX |
| 9 | 1268 | Erzincan | IX | 21 | 1701 | Van | VIII | 33 | 1881 | Van-Bitlis | IX |
| 10 | 1276 | Ahlat-Van | VIII | 22 | 1715 | Van -Erçiş | VIII | 34 | 1890 | Erzincan | IX |
| 11 | 1319 | Ağrı | VIII | 23 | 1784 | Erzincan | VIII | 35 | 1891 | Muş-Bitlis | VIII |
| 12 | 1363 | Muş | IX | 24 | 1789 | Elazığ | VIII | 36 | 1893 | Malatya | IX |

Significant instrumental period earthquakes that occurred in the region are given in Table 2 [57–64]. In Turkey, the most destructive and largest earthquake occurred in 1939 (Erzincan, Mw = 7.9), and about 33,000 people were killed. A total of 232,549 damaged buildings also shows the seismic hazard in the region.

**Table 2.** Significant instrumental period earthquakes in the Eastern Anatolian Region.

| No | Date | Region | MMI Io | Mw | Loss of Life | Damaged Buildings | No | Date | Region | MMI Io | Mw | Loss of Life | Damaged Buildings |
|---|---|---|---|---|---|---|---|---|---|---|---|---|---|
| 1 | 1901 | Erzurum | VIII | 6.1 | 500 | 10,000 | 26 | 1988 | Kars | X | 6.9 | 4 | 546 |
| 2 | 1903 | Muş | IX | 6.7 | 600 | 450 | 27 | 1992 | Erzincan | VIII | 6.8 | 653 | 8057 |
| 3 | 1905 | Malatya | IX | 6.8 | 500 | 5000 | 28 | 1992 | Tunceli | VII | 5.8 | | 439 |
| 4 | 1906 | Kars | | 6.2 | | | 29 | 1995 | Tunceli | VI+ | 5.7 | 1 | |
| 5 | 1908 | Van | | 6.3 | | | 30 | 1998 | Bingöl | VI | 5 | | 148 |
| 6 | 1924 | Erzurum | IX | 6.8 | 60 | 380 | 31 | 2003 | Tunceli | VII | 6.2 | 1 | 50 |
| 7 | 1926 | Kars | VIII | 5.9 | 3 | 2043 | 32 | 2003 | Bingöl | VIII | 6.4 | 176 | 6000 |
| 8 | 1930 | Hakkari | X | 7.2 | 2514 | 3000 | 33 | 2004 | Erzurum | VII | 5.6 | 9 | 1280 |
| 9 | 1939 | Erzincan | VII | 5.9 | 43 | 500 | 34 | 2004 | Ağrı | VII | 5.1 | 17 | 1000 |
| 10 | 1939 | Erzincan | X-IX | 7.9 | 32,968 | 116,720 | 35 | 2004 | Elazığ | VII | 5.9 | | |
| 11 | 1941 | Van | VIII | 5.9 | 192 | 600 | 36 | 2005 | Hakkari | VII | 5.9 | 3 | 82 |
| 12 | 1941 | Erzincan | VIII | 5.9 | 15 | 600 | 37 | 2005 | Bingöl | VI | 5.7 | | |
| 13 | 1946 | Muş | VIII | 5.9 | 839 | 3000 | 38 | 2005 | Bingöl | VII | 5.9 | | 760 |
| 14 | 1949 | Bingöl | IX | 6.7 | 450 | 3500 | 39 | 2005 | Bingöl | VI | 5.7 | | |
| 15 | 1952 | Erzurum | VIII | 5.8 | 41 | 701 | 40 | 2005 | Bingöl | VI | 5.7 | | |

**Table 2.** *Cont.*

| No | Date | Region | MMI Io | Mw | Loss of Life | Damaged Buildings | No | Date | Region | MMI Io | Mw | Loss of Life | Damaged Buildings |
|---|---|---|---|---|---|---|---|---|---|---|---|---|---|
| 16 | 1964 | Malatya | VIII | 6 | 8 | 847 | 41 | 2007 | Elazığ | VI | 5.5 | | |
| 17 | 1966 | Muş | VIII | 5.6 | 14 | 1100 | 42 | 2007 | Elazığ | VII | 5.9 | | |
| 18 | 1966 | Muş | IX | 6.9 | 2396 | 20,007 | 43 | 2010 | Elazığ | VII | 6.1 | 42 | |
| 19 | 1967 | Tunceli | VIII | 5.9 | 97 | 1282 | 44 | 2010 | Elazığ | VI | 5.6 | | |
| 20 | 1971 | Bingöl | VIII | 6.8 | 878 | 9111 | 45 | 2011 | Erzincan | VI | 5.6 | | |
| 21 | 1976 | Van | IX | 7.5 | 3840 | 9232 | 46 | 2011 | Van | VIII | 7.2 | 644 | 17,005 |
| 22 | 1983 | Erzurum | VIII | 6.9 | 1155 | 3241 | 47 | 2011 | Van | VI | 5.6 | | |
| 23 | 1984 | Erzurum | VIII | 6.4 | 3 | 570 | 48 | 2011 | Van | VI | 5.6 | 40 | |
| 24 | 1986 | Malatya | VIII | 5.9 | 7 | 824 | 49 | 2020 | Elazığ | | 6.8 | 41 | 3300 |
| 25 | 1986 | Malatya | VIII | 5.6 | 1 | 1174 | 50 | 2020 | Van | | 6.0 | 9 | |

## 3. Distribution of Seismic Moments in Eastern Anatolia

The process of energy accumulation and release is known as the seismic activity. The seismic moment (Mo) is a measure used to calculate the energy released during an earthquake and is defined as the physical moment of forces at the earthquake source. The characteristic Mo accumulation and oscillation model follows the energy balance principle and assumes that the moment produced by an earthquake is equal to the accumulation along a seismic fault over a recurrence interval. It is also one of the basic parameters characterizing the magnitude of an earthquake [65]. The Mo, which considers the magnitude of the earthquake in terms of displacement phenomenon, has been accepted as the most useful measure [66]. The moment magnitude (Mw) derived from the static seismic moment is a measure of an earthquake, namely the average tectonic effect of an earthquake. The Mo depends on the difference in energy of the stress before and after the earthquake. It is largely controlled by the dynamic and kinematic properties of the rupture process, and therefore it is extremely important to assess the true damage potential associated with the seismic energy released from an earthquake [67]. The Mo measurement is used to predict seismic stress and stress drops occurring at a focal point [68]. It acts as the average of the tectonic conditions, earthquake energy accumulation, and resource properties of a region. The Mo in numerically recorded earthquakes is usually estimated from seismograms. In addition, it can be calculated by converting from different types of earthquake magnitudes through the formulas developed by different researchers. The most commonly used formulas were developed by Hanks and Kanomori (1979) [69]. The relationship between the Mo and body wave magnitude (mb) is given below:

$$\log Mo = 1.36 m_b + 17.24 \quad (1)$$

Similarly, the relationship between the local magnitude ($M_L$) and the Mo is given as follows:

$$\log Mo = 1.5 M_L + 16.0 \quad (2)$$

The transformation from Mw is defined below:

$$\log Mo = 1.5 M_w + 9.045 \quad (3)$$

The following equations were developed between the magnitude of the surface wave (Ms) and Mo according to different Ms value ranges [48]:

$$\log Mo = 1.5 M_s + 16.4 \text{ for } Ms > 6.8 \quad (4)$$

$$\log Mo = 30.2 - (92.45 - 11.4M_s)^{0.5} \text{ for } 5.3 < Ms < 6.8 \quad (5)$$

$$\log Mo = M_s + 19.24 \text{ for } Ms > 5.3 \quad (6)$$

Here, we produced an image map to obtain the distribution of Mo in the region (Figure 4). The distributions of the earthquake epicenters are also shown on the map. Large and destructive earthquakes in Eastern Anatolia showed high Mo values, as expected. Earthquakes with magnitudes of 6.0 or more were mostly recorded in the catalogue according to the Ms. The Erzincan earthquake, which is the largest one in the region (1939, Mw = 7.9), showed less Mo distribution than the Çaldıran (Van) earthquake (1976, Mw = 7.6). This low distribution is due to the fact that such a large earthquake has not occurred in the province of Erzincan or its surroundings so far. The map also shows that the highest Mo distribution existing in the region between the Van and Hakkari provinces. The region between these provinces has a much higher energy accumulation, and the recurrence period of large earthquakes is much shorter. It is inevitable for the seismic moment distribution to attain high values. In addition, almost every province showed high Mo distribution. This finding also indicates the high seismic risk in the Eastern Anatolian Region. It can be seen that the Mo reached higher values in destructive earthquakes, and this showed a linear change with the released energy.

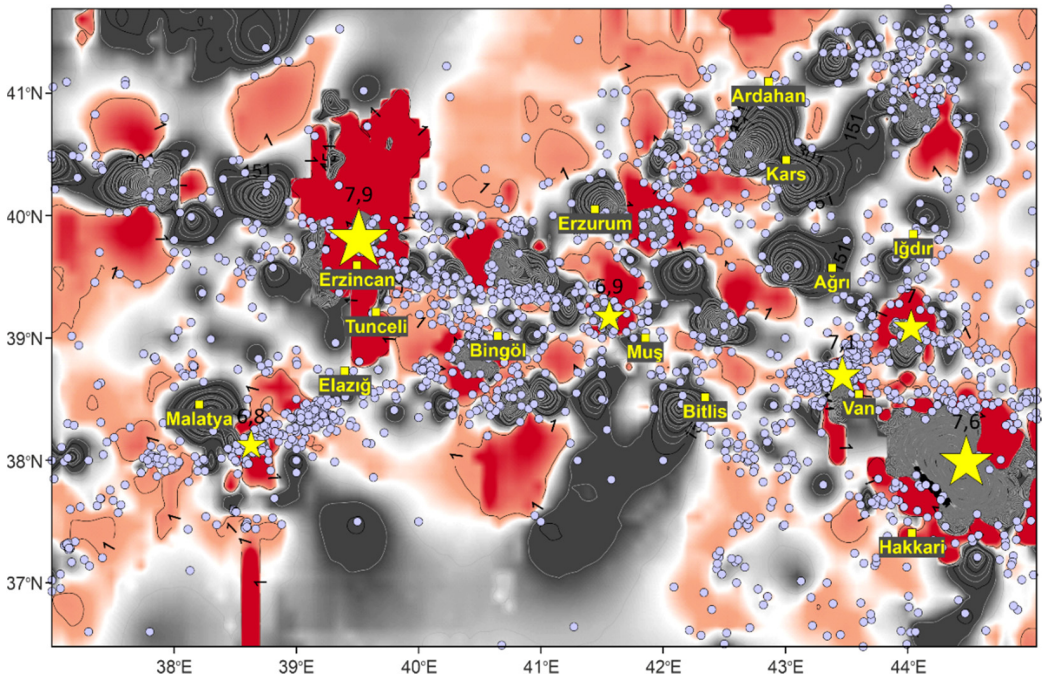


**Figure 4.** Distribution of logMo in Eastern Anatolia. Red (low) and gray (high) counters present the Mo intensity distribution. Small circles represent epicenters. Yellow-colored stars show major earthquakes between 6.8 and 7.9 in the region. The magnitudes of the earthquakes are shown above the yellow-colored stars.

## 4. Seismic Hazard Analysis

The annual exceedance probability of the design level PGA suggested in [70] was used for seismic risk analyses. Probabilistic seismic hazard analyses define the seismic sources, formation rates for the size distribution and sources, formation of ground motion, and finally involve probability analysis. Here, all provincial centers in the region were used for analysis. Only the earthquake ground motion level with a probability of exceedance of 10% in 50 years and a reputation period of 475 years was defined in the previous seismic design code. On the other hand, the ground motion levels were defined in four different types in the updated code. Here, these levels were considered for seismic hazard analysis

by using the updated TBEC-2018 [31] (Table 3). The PGA, PGV, $S_S$, and $S_1$ were obtained separately for different probabilities of exceedance in 50 years from the Turkish Earthquake Hazard Map Interactive Web Application for each province (Tables 4 and 5). The PGA values were in the range of 0.38–1.14 g for 2%, 0.2–0.65 g for 10%, 0.076–0.28 g for 50%, and 0.055–0.18 g for 68% probabilities of exceedance in the region. It is clearly seen that the highest and lowest parameter values were obtained in the Bingöl and Kars provinces, respectively. Additionally, the Erzincan and Erzurum provinces were also characterized by high values.

**Table 3.** Earthquake ground motion levels [31].

| Earthquake Level | Repetition Period (Year) | Probability of Exceedance (in 50 Years) | Description |
|---|---|---|---|
| DD-1 | 2475 | 0.02 | Largest earthquake ground motion |
| DD-2 | 475 | 0.10 | Standard design earthquake ground motion |
| DD-3 | 72 | 0.50 | Frequent earthquake ground motion |
| DD-4 | 43 | 0.68 | Service earthquake movement |

**Table 4.** PGA and PGV values for different probabilities of exceedance in 50 years.

| Province | PGA (g) | | | | PGV ($ms^{-2}$) | | | |
|---|---|---|---|---|---|---|---|---|
| | Probability of Exceedance in 50 Years | | | | Probability of Exceedance in 50 Years | | | |
| | 2% | 10% | 50% | 68% | 2% | 10% | 50% | 68% |
| Ağrı | 0.451 | 0.234 | 0.091 | 0.066 | 25.925 | 13.640 | 5.798 | 4.313 |
| Ardahan | 0.520 | 0.269 | 0.098 | 0.068 | 29.926 | 14.694 | 5.608 | 4.114 |
| Bingöl | 1.136 | 0.654 | 0.275 | 0.179 | 77.511 | 43.563 | 15.636 | 9.588 |
| Bitlis | 0.490 | 0.260 | 0.106 | 0.077 | 28.200 | 15.065 | 6.506 | 4.847 |
| Elazığ | 0.717 | 0.386 | 0.179 | 0.100 | 46.493 | 24.215 | 9.026 | 5.903 |
| Erzincan | 1.092 | 0.597 | 0.216 | 0.147 | 74.271 | 39.230 | 12.859 | 8.353 |
| Erzurum | 0.877 | 0.477 | 0.152 | 0.098 | 54.049 | 28.780 | 9.455 | 6.033 |
| Hakkari | 0.600 | 0.318 | 0.116 | 0.079 | 34.001 | 16.676 | 5.977 | 4.209 |
| Iğdır | 0.481 | 0.245 | 0.089 | 0.062 | 27.052 | 13.269 | 5.414 | 3.923 |
| Kars | 0.379 | 0.195 | 0.076 | 0.055 | 21.765 | 11.442 | 4.900 | 3.75 |
| Malatya | 0.654 | 0.348 | 0.136 | 0.092 | 41.267 | 21.446 | 8.054 | 5.365 |
| Muş | 0.579 | 0.327 | 0.138 | 0.098 | 35.589 | 20.461 | 8.609 | 5.989 |
| Tunceli | 0.672 | 0.348 | 0.128 | 0.087 | 42.198 | 21.992 | 8.393 | 5.685 |
| Van | 0.516 | 0.271 | 0.100 | 0.069 | 29.756 | 15.224 | 5.941 | 4.303 |

The spectral acceleration coefficient ($S_{DS}$) was calculated on a regional basis in the previous code. However, it was obtained by using site-specific analysis in the updated code. A comparison between these two codes was performed with $S_{DS}$ for the design earthquake (DD-2) with a 10% probability of exceedance per 50 years (Table 6). It was observed that some of the studied provinces produced the same coefficient values through the previous code, but very different values were obtained for the provinces when using the updated code. Therefore, site-specific analysis caused the seismic parameters obtained for each province to differ from each other, as expected. This finding reveals the importance of microzonation once again.

**Table 5.** $S_S$ and $S_1$ values for different probabilities of exceedance in 50 years.

| Province | Short Period Map Spectral Acceleration Coefficient ($S_S$) | | | | Map Spectral Acceleration Coefficient for the Period of 1.0 Seconds ($S_1$) | | | |
|---|---|---|---|---|---|---|---|---|
| | Probability of Exceedance in 50 Years | | | | Probability of Exceedance in 50 Years | | | |
| | 2% | 10% | 50% | 68% | 2% | 10% | 50% | 68% |
| Ağrı | 1.084 | 0.549 | 0.210 | 0.151 | 0.279 | 0.152 | 0.065 | 0.049 |
| Ardahan | 1.249 | 0.624 | 0.222 | 0.155 | 0.308 | 0.153 | 0.060 | 0.044 |
| Bingöl | 2.873 | 1.606 | 0.644 | 0.423 | 0.802 | 0.421 | 0.155 | 0.095 |
| Bitlis | 1.192 | 0.613 | 0.243 | 0.176 | 0.311 | 0.172 | 0.076 | 0.055 |
| Elazığ | 1.747 | 0.920 | 0.346 | 0.230 | 0.502 | 0.260 | 0.098 | 0.064 |
| Erzincan | 2.709 | 1.434 | 0.497 | 0.333 | 0.832 | 0.413 | 0.133 | 0.085 |
| Erzurum | 2.181 | 1.134 | 0.350 | 0.226 | 0.564 | 0.294 | 0.102 | 0.066 |
| Hakkari | 1.484 | 0.749 | 0.268 | 0.183 | 0.362 | 0.180 | 0.066 | 0.046 |
| Iğdır | 1.157 | 0.571 | 0.206 | 0.144 | 0.280 | 0.147 | 0.060 | 0.043 |
| Kars | 0.895 | 0.449 | 0.171 | 0.123 | 0.238 | 0.129 | 0.056 | 0.042 |
| Malatya | 1.594 | 0.830 | 0.314 | 0.213 | 0.440 | 0.229 | 0.085 | 0.056 |
| Muş | 1.449 | 0.794 | 0.320 | 0.226 | 0.402 | 0.230 | 0.098 | 0.066 |
| Tunceli | 1.640 | 0.827 | 0.298 | 0.203 | 0.454 | 0.240 | 0.095 | 0.064 |
| Van | 1.267 | 0.639 | 0.227 | 0.159 | 0.312 | 0.163 | 0.066 | 0.048 |

**Table 6.** The comparison of spectral acceleration coefficients with different ground types. DD-2: the earthquake ground motion level; ZA: soil type with solid hard rocks; ZE: soil type with loose sand, gravel, or soft clay-solid clay layers.

| DD-2 | ZA | | ZE | | All Ground Types | |
|---|---|---|---|---|---|---|
| Settlements | TBEC-2018 | | TBEC-2018 | | TSDC-2007 | |
| | $S_{DS}$ | $0.40S_{DS}$ | $S_{DS}$ | $0.40S_{DS}$ | $S_{DS}$ | $0.40S_{DS}$ |
| Ağrı | 0.439 | 0.176 | 0.890 | 0.356 | 0.75 | 0.3 |
| Ardahan | 0.499 | 0.200 | 0.937 | 0.3748 | 0.75 | 0.3 |
| Bingöl | 1.285 | 0.514 | 1.285 | 0.514 | 1 | 0.4 |
| Bitlis | 0.490 | 0.196 | 0.931 | 0.3724 | 1 | 0.4 |
| Elazığ | 0.736 | 0.294 | 1.071 | 0.4284 | 0.75 | 0.3 |
| Erzincan | 1.147 | 0.459 | 1.185 | 0.474 | 1 | 0.4 |
| Erzurum | 0.907 | 0.363 | 1.126 | 0.4504 | 0.75 | 0.3 |
| Hakkari | 0.599 | 0.240 | 0.975 | 0.39 | 1 | 0.4 |
| Iğdır | 0.457 | 0.183 | 0.906 | 0.3624 | 0.75 | 0.3 |
| Kars | 0.359 | 0.144 | 0.827 | 0.3308 | 0.75 | 0.3 |
| Malatya | 0.664 | 0.266 | 1.026 | 0.4104 | 1 | 0.4 |
| Muş | 0.635 | 0.254 | 1.004 | 0.4016 | 1 | 0.4 |
| Tunceli | 0.662 | 0.265 | 1.024 | 0.4096 | 0.75 | 0.3 |
| Van | 0.511 | 0.204 | 0.944 | 0.3776 | 0.75 | 0.3 |

Generally, the seismicity characteristics include some parameters such as faults or fault groups, the properties of the faults, the distance of structures from the fault, the earthquake history of the region, and the properties of previous earthquakes. In addition to these parameters, it is a well-known fact that local soil conditions directly affect the seismic behavior of structures and also modify the reference seismic hazard coefficients defined for the outcropping rock environment. Moreover, the building stock in the region is particularly important in terms of the damage and loss of life that may occur as a result of the earthquake.

The adobe stone masonry style is widely used and generally consists of 1–2 floors, especially in rural areas in the Eastern Anatolian Region. Such masonry structures are built by local craftsmen and workers using local materials without any engineering service. The walls are used as carrier system elements, and they are built in a thick form in the masonry building stocks. These buildings, which are easy to build from local materials, are preferred due to economical reasons. Soil drips are generally used in the top covers of such structures. Thus, the earthquake performances of these large masses are quite low. The damages in these structures caused by earthquakes clearly reveal this situation in the region. Most of the buildings in the region are built by medium-height reinforced concrete (RC) structures together with the masonary structures. However, instead of these buildings, high-rise RC buildings started to be used in recent years. Steel and prefabricated structures are generally used in shopping malls and industrial structures.

The interaction between the seismicity characteristics and local soil conditions is used for structural analysis. Earthquake design spectra obtained from different probabilities of exceedances can be used in this analysis. Differences in the design spectra significantly affect the target displacement in structural analysis. Structures which do not meet the target displacement demands at high values are clearly distant from the true values for the damage estimates and building performance. More accurate determination of the local soil conditions and regional seismicity generally provides more realistic building designs and assessments [71–73]. Ground motion amplification to account for local soil and site effects is established through a constant soil factor, which uniformly increases the normalized elastic response spectra in all periods [74].

In the previous seismic design code, soil classes and soil groups were expressed only as local soil classes together with the updated code, and six different local soil classes were expressed. Here, an average local soil type was selected as the ZC type given in TBEC-2018 (very dense sand, gravel, hard clay layers, or weathered rocks with many cracks) [31] to make comparisons. The characteristics of this soil type (ZC) are given in Table 7.

**Table 7.** Local soil class type ZC [31].

| Local Soil Class | Soil Type | Upper Average at 30 m | | |
|---|---|---|---|---|
| | | $(V_S)_{30}$ (m/s) | (N60)30 (Pulse/30 cm) | (cu)30 (kPa) |
| ZC | Very tight sand, gravel, and hard clay layers or weathered, very cracked weak rocks | 360–760 | 50 | 250 |

Local ground coefficients ($F_s$ and $F_1$) were used for the first time with the current code. The local soil effect coefficient $F_S$ and local soil effect coefficient for a 1.0-s period ($F_1$) for the ZC soil type are given in Tables 8 and 9, respectively.

**Table 8.** Local soil coefficient $F_S$ for the short period zone for ZC [31].

| Local Soil Class | Local Ground Effect Coefficients ($F_s$) for ZC Class | | | | | |
|---|---|---|---|---|---|---|
| | $S_S \leq 0.25$ | $S_S = 0.50$ | $S_S = 0.75$ | $S_S = 1.00$ | $S_S = 1.25$ | $S_S \geq 1.50$ |
| ZC | 1.30 | 1.30 | 1.20 | 1.20 | 1.20 | 1.20 |

**Table 9.** Local soil effect coefficients for class ZC ($F_1$) [31].

| Local Soil Class | Local Ground Effect Coefficients ($F_1$) for 1.0 s Period | | | | | |
|---|---|---|---|---|---|---|
| | $S_1 \leq 0.10$ | $S_1 = 0.20$ | $S_1 = 0.30$ | $S_1 = 0.40$ | $S_1 = 0.50$ | $S_1 \geq 0.60$ |
| ZC | 1.50 | 1.50 | 1.50 | 1.50 | 1.50 | 1.40 |

The horizontal and vertical elastic design spectra were obtained for various recurrence periods in each province. Here, the amplification factor of the soil was assumed to be constant (~1.5). However, soil nonlinearity plays an important role in defining soil factors, especially in soft soils. The amplification of soft soils is higher than that of hard soils. The soil type and soil nonlinearity affect the definition of seismic hazards and the response of the structure [75]. The presence of soil nonlinearity highlights the inaccuracy of using constant soil factors for sites with different seismic hazards [76]. Probabilistic seismic hazard analyses are usually performed with quasi-experimental ground motion models from global databases, where the average source, path, and site effects are valid for a particular area of interest. The site-specific site response differs from the global average based on the seismic velocity and basin depth field parameters used in ground motion models [77]. The comparison of the horizontal and vertical elastic design spectra obtained are shown in Figures 5 and 6, respectively. Unlike the previous seismic design code, vertical elastic design spectra were used with a horizontal one in the updated code. Therefore, the effects of the earthquake were considered in both directions.

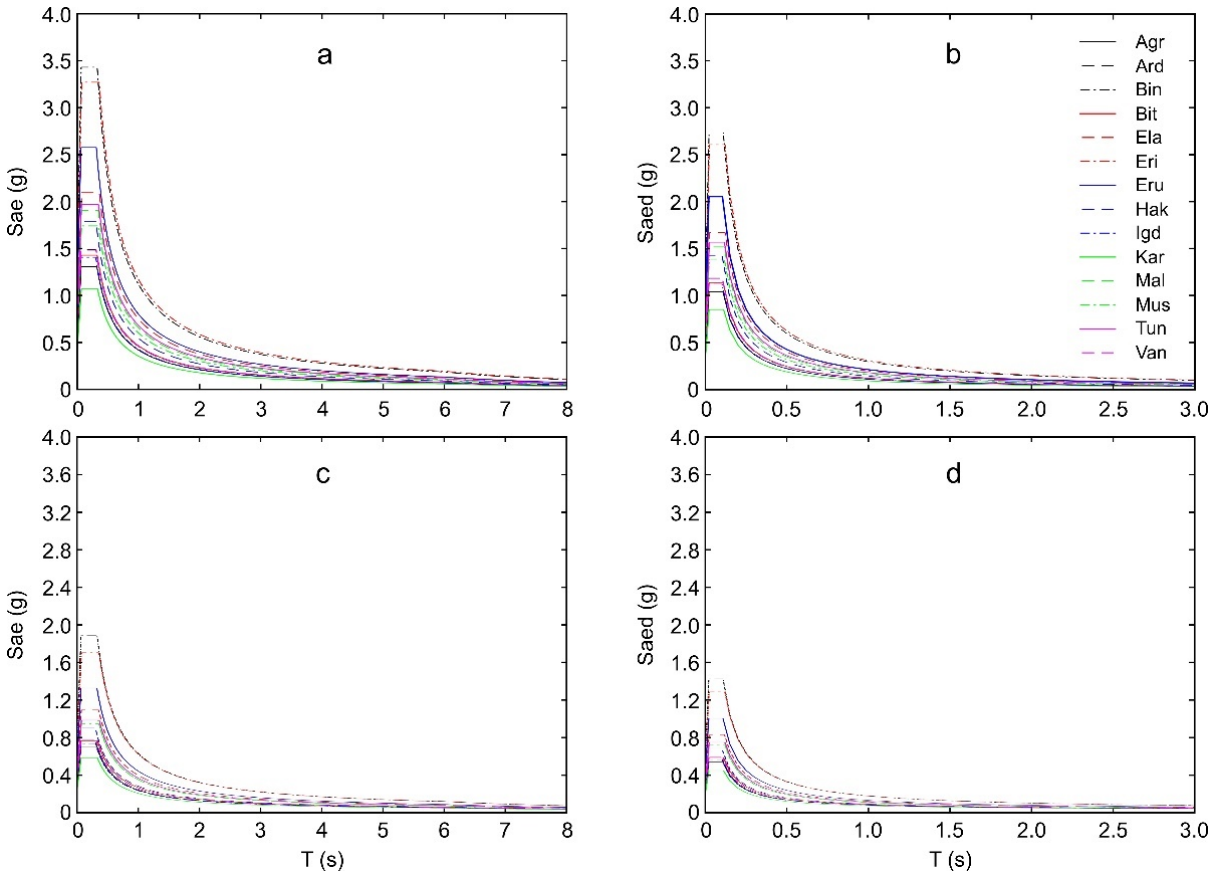


**Figure 5.** (**a**) Horizontal and (**b**) vertical elastic design spectra for 2% probability of exceedance in 50 years. (**c**) Horizontal and (**d**) vertical elastic design spectra for 10% probability of exceedance in 50 years.

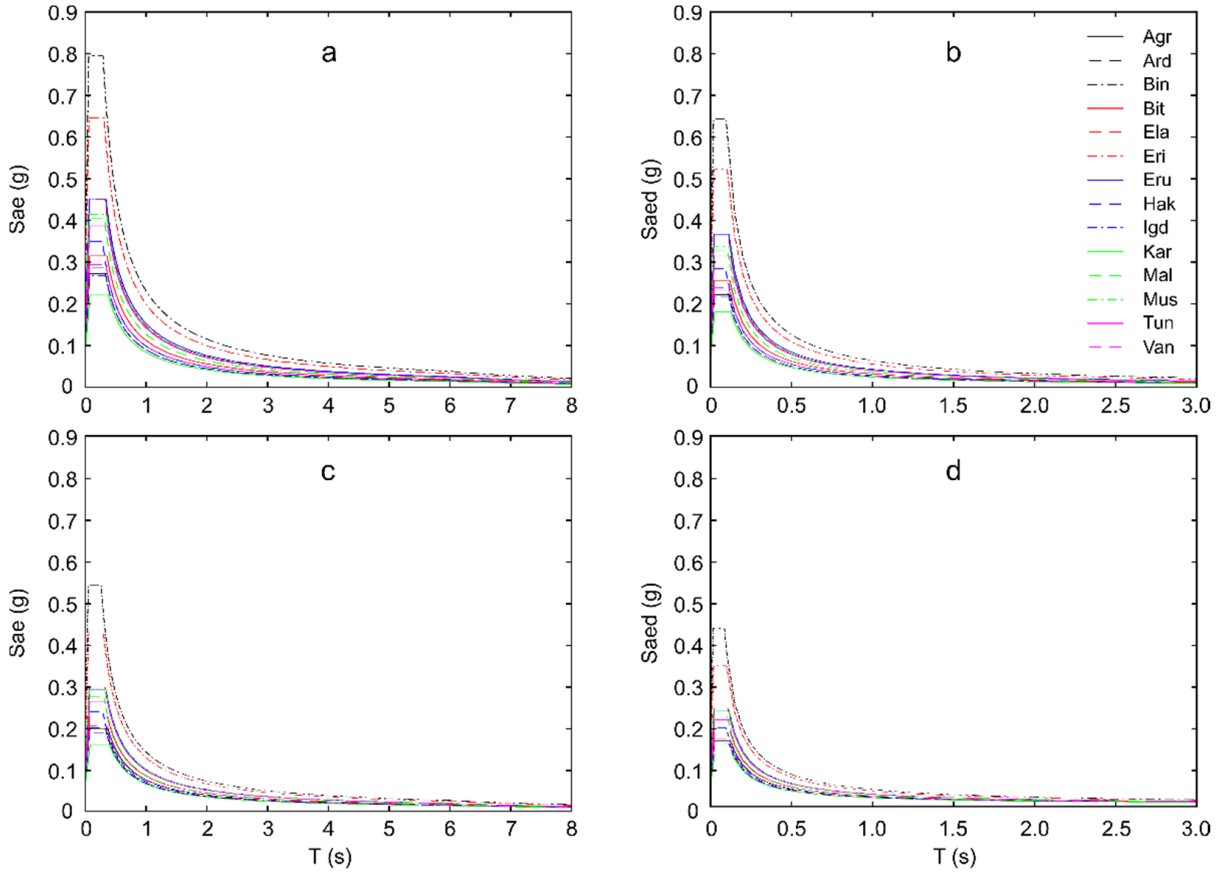


**Figure 6.** (**a**) Horizontal and (**b**) vertical elastic design spectra for 50% probability of exceedance in 50 years. (**c**) Horizontal and (**d**) vertical elastic design spectra for 68% probability of exceedance in 50 years.

As mentioned before and seen from the design spectra, the Bingöl province has the highest risk in the studied region. Thus, we compared the spectra with different probabilities of exceedance in 50 years, which are defined in TBEC-2018 (Figure 7). Although there were some differences in the spectral acceleration values, similar curve characteristics were obtained for other provinces. The magnitude of the expected earthquake increased when the probability of exceedance decreased. Figure 8 shows various probabilities of exceedance in 50 years for the region obtained by using the PGA values.

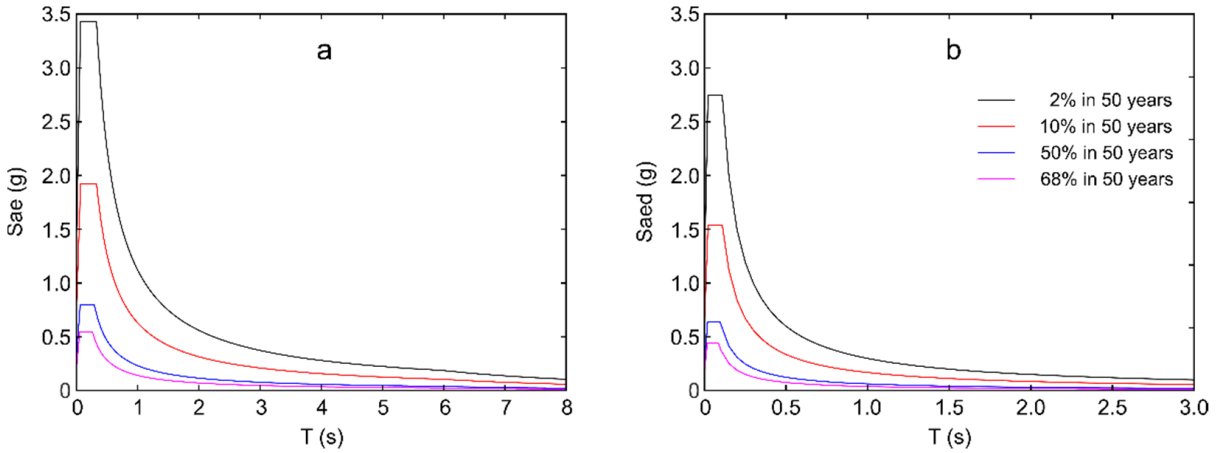


**Figure 7.** The comparison of the horizontal and vertical elastic design spectra for various probabilities of exceedance 50 years for Bingöl: (**a**) horizontal and (**b**) vertical.

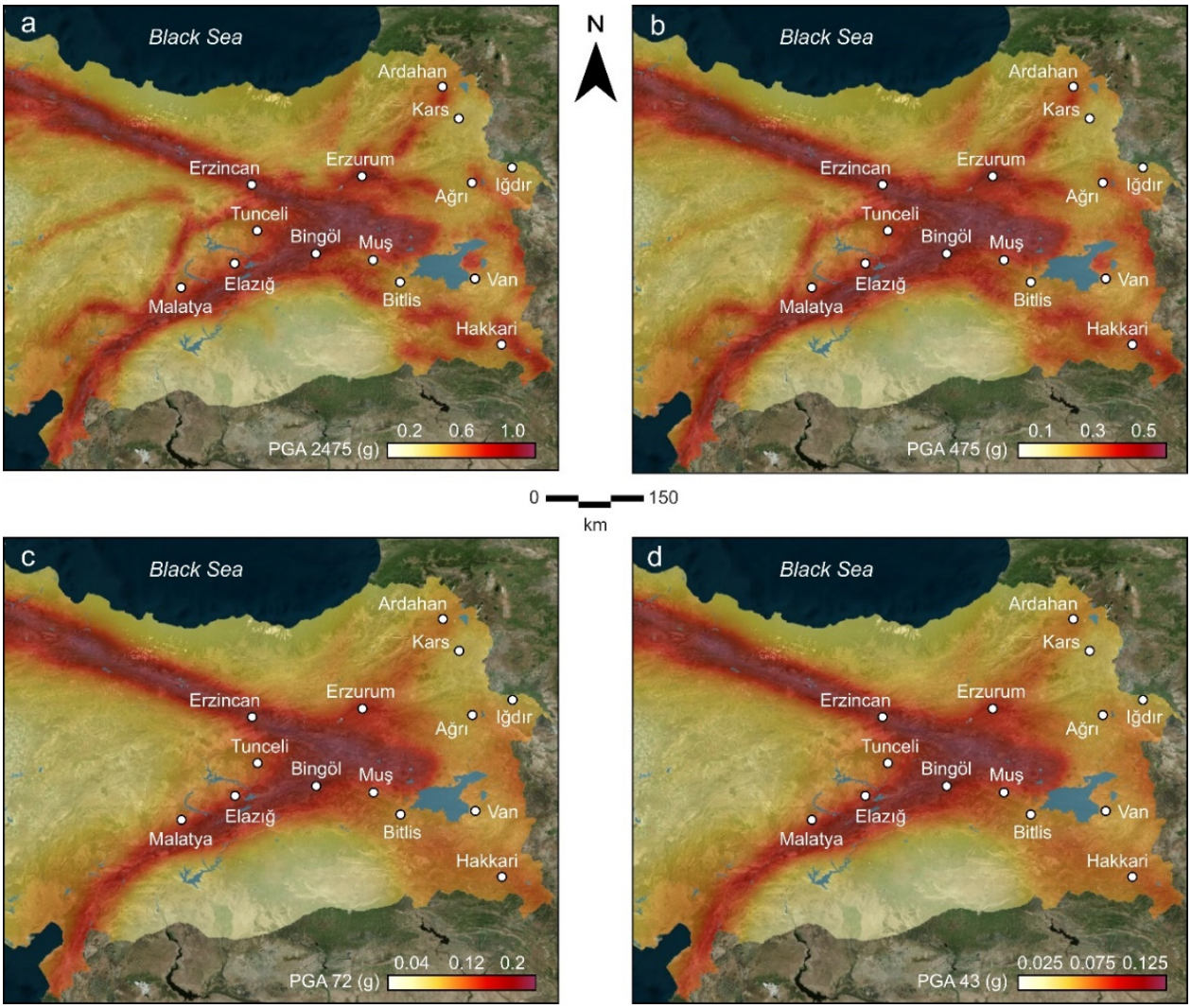


**Figure 8.** Seismic hazard maps for different probabilities of exceedance in 50 years: (**a**) 2%, (**b**) 10%, (**c**) 50%, and (**d**) 68%.

In the region, there are limited records for strong ground motion accelerations. Additionally, there is no attenuation relationship specific to the region. Therefore, as seen from Figure 9, we performed seismic hazard analysis for the Bingöl province using six worldwide applicable empirical attenuation relationships [78–83]. The spectra curve obtained by means of the updated code did not fit well with the other ones. However, it did not reach the upper or lower bounds of the other curves for different probabilities of exceedance. This finding clearly indicates that the attenuation relationship to be used should be obtained from the studied region.

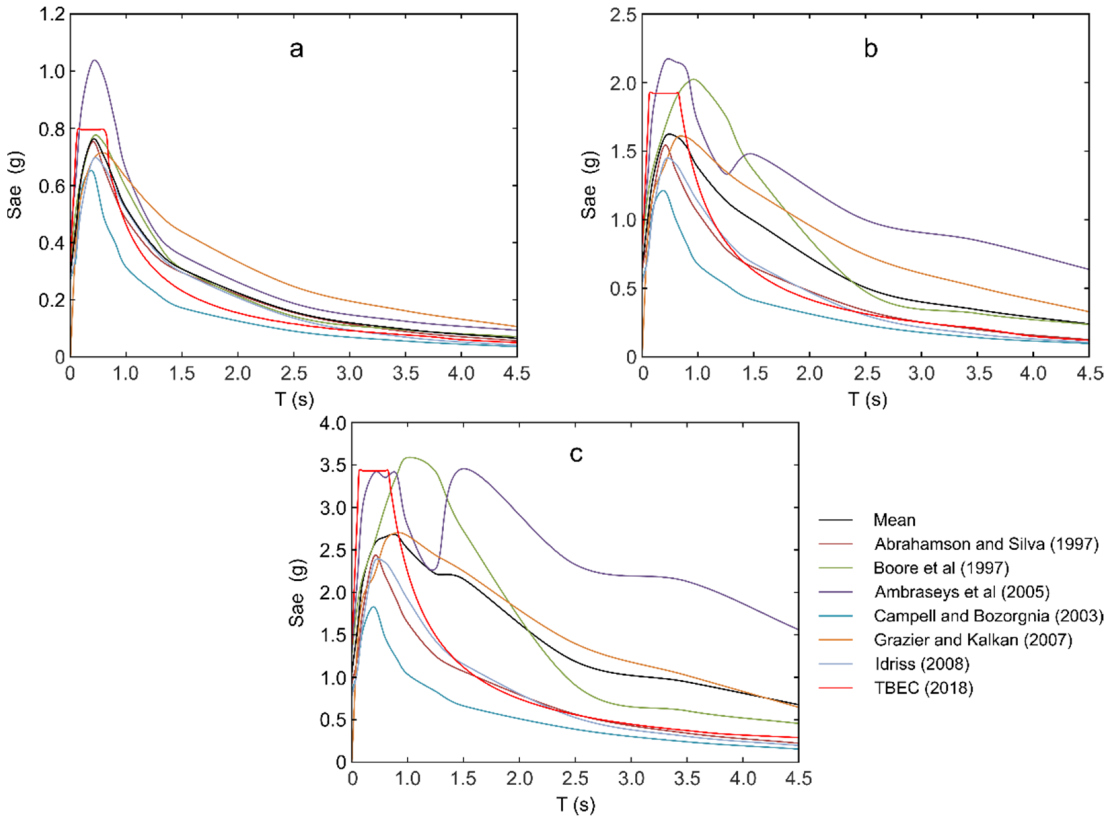


**Figure 9.** Comparison of spectral responses for the return period (**a**) for 72 years, (**b**) for 475 years, and (**c**) for 2475 years in Bingöl province.

## 5. Comparison of Structural Analyses under Different Earthquake Ground Motion Levels

We used Seismostruct software [84] to perform structural analysis with different probabilities of exceedance for the Bingöl province. The structural elements were discretized using beam–column models based on the fiber element approach [85]. Adaptive pushover analysis applied in estimating the horizontal capacity of a structure was used, taking into account the effect of the deformation and the frequency content of the input motion on the dynamic response properties. Analyses were performed by considering the mode shapes and participation factors obtained from the eigenvalue analyses in each step during the adaptive pushover analysis [86–89]. We modeled an RC building with seven stories. Additionally, the same structural characteristics for each probability of exceedance were used. The ZC soil type was selected as local soil condition. The PGA value and design spectrum obtained specifically for each earthquake ground motion level were selected as the variables. The base shear forces, displacements, stiffness values, and limit states were obtained. As the selected building model was symmetrical, analyses were carried out in only one direction. The damping ratio and important class were set to 5% and IV, respectively. The nonlinear concrete model [90] and steel model [91] were used for concrete and steel material. Figure 10 shows the stress–strain relationship of the material models. The blueprint of the sample model is given in Figure 11. The two- and three-dimensional structural models and the applied loads to the building are shown in Figure 12. We used incremental load values as the displacement load and a permanent load value of 5.00 kN. The value of 0.42 m was selected for the target displacement. The story heights were 3 m in the building.

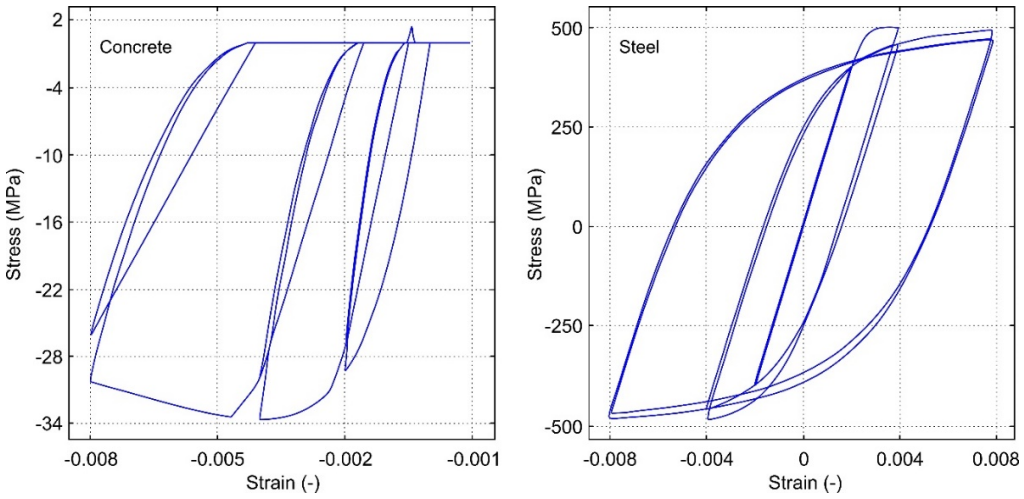


**Figure 10.** Material models for concrete and steel considered in the study [74].

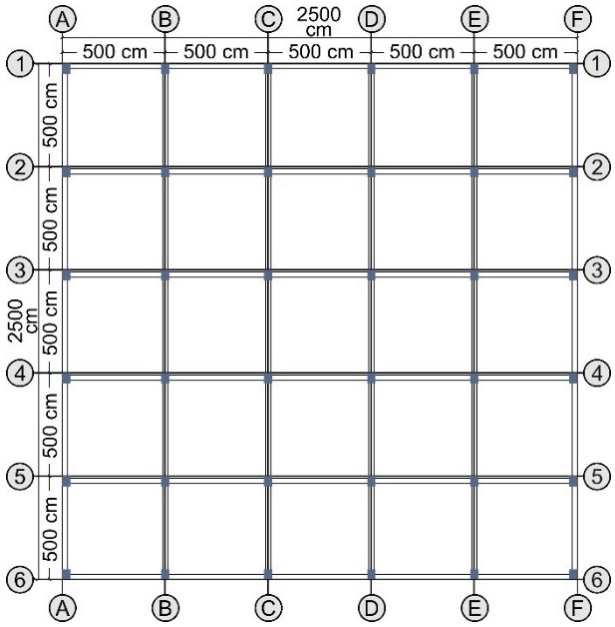


**Figure 11.** Blueprint of the sample reinforced concrete (RC) building.

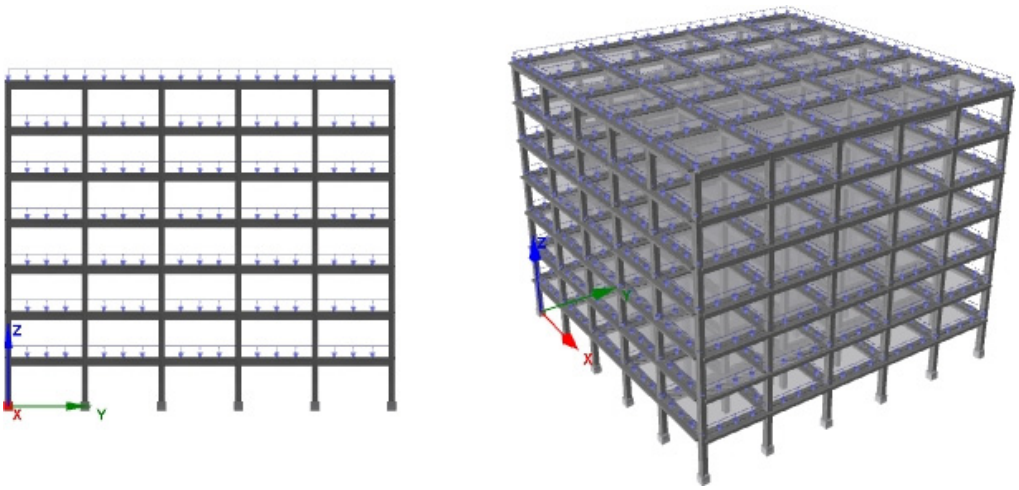

**Figure 12.** Two- and three-dimensional models of the selected 7-story RC building.

C25-S420 was selected as the material grade for the sample model. The transverse reinforcements were set to ϕ10/10 in the columns and ϕ10/15 in the beams. The reinforcements used in all columns were selected to be 4ϕ20 in the corners, 4ϕ16 at the top and bottom, and 4ϕ16 on the left and right sides. The reinforcements used in all beams were selected to be 4ϕ16 at the lower end, 5ϕ18 at the upper end, 2ϕ12 at the sides, 4ϕ10 in the lower slab, and 6ϕ10 in the upper slab. Figure 13 shows the column and beam cross-sections used in the sample model. The model was analyzed with horizontal design spectrum curves obtained from different earthquake ground motion levels for the Bingöl province.

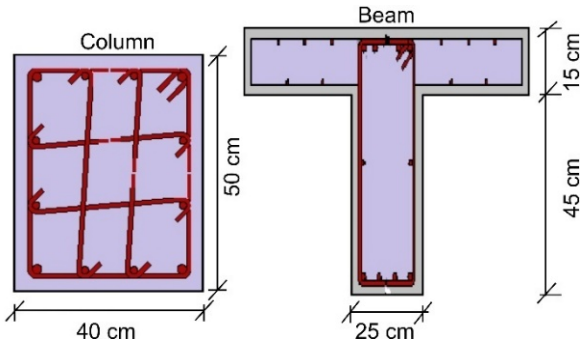


**Figure 13.** Column and beam cross-sections.

While modeling the structural models, force-based plastic hinge frame members (infrmFBPH) were used for the columns and beams. These element models distributed inelasticity based on force and only constrained the plasticity to a finite length. The ideal number of fibers in the cross-section should be sufficient to model the stress–strain distribution in the cross-section [92]. One hundred fiber elements were defined for the selected structural sections. This value was sufficient for such sections.

We obtained the displacements for three different points on the idealized curve. The yield displacement ($d_y$) was the first point. The intermediate displacement ($d_{int}$) and the target (or ultimate) displacement ($d_t$) were the second and third points on the curve, respectively. The elastic stiffness value (K_elas) and effective stiffness (K_eff) for each earthquake ground motion level were directly calculated via the stiffness reduction coefficients predicted. The target displacements for damage estimation must be determined for the performance limits of structural elements in performance-based earthquake engineering. In this study, we used the limit states which are defined in Eurocode-8 (Part 3) [93,94]. Table 10 gives the limit states for damage estimation in this code. Typical pushover and idealized curves as well as the calculated displacements are demonstrated in Figure 14.

**Table 10.** Limit states in Eurocode 8 (Part 3) [93,94].

| Limit State | Description | Return Period (Year) | Probability of Exceedance (in 50 Years) |
|---|---|---|---|
| Limit state of damage limitation (DL) | Only lightly damaged, damage to non-structural components economically repairable | 225 | 0.20 |
| Limit state of significant damage (SD) | Significantly damaged, some residual strength and stiffness, non-structural components damaged, uneconomic to repair | 475 | 0.10 |
| Limit state of near collapse (NC) | Heavily damaged, very low residual strength and stiffness, large permanent drift but still standing | 2475 | 0.02 |

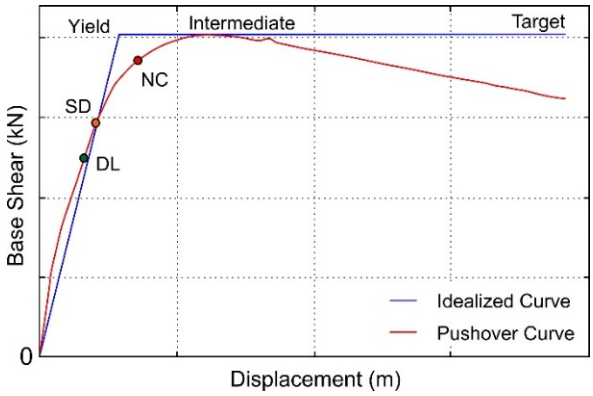


**Figure 14.** Typical pushover and idealized curves and calculated displacements.

Table 11 shows all target displacements obtained in the X direction in the sample RC building for all provinces in the region according to the last two seismic design codes. The DD-2 ground motion level was selected for comparison with the previous code.

**Table 11.** Comparisons of target displacements.

| Provinces | Code | Target Displacements (m) | | |
|---|---|---|---|---|
| | | DL | SD | NC |
| Ağrı | TBEC-2018 | 0.106 | 0.137 | 0.237 |
| Ardahan | | 0.122 | 0.157 | 0.272 |
| Bingöl | | 0.298 | 0.382 | 0.662 |
| Bitlis | | 0.118 | 0.152 | 0.263 |
| Elazığ | | 0.176 | 0.225 | 0.390 |
| Erzincan | | 0.270 | 0.347 | 0.601 |
| Erzurum | | 0.217 | 0.278 | 0.482 |
| Hakkari | | 0.145 | 0.186 | 0.322 |
| Iğdır | | 0.111 | 0.143 | 0.248 |
| Kars | | 0.089 | 0.114 | 0.197 |
| Malatya | | 0.158 | 0.203 | 0.352 |
| Muş | | 0.149 | 0.191 | 0.331 |
| Tunceli | | 0.158 | 0.203 | 0.352 |
| Van | | 0.123 | 0.158 | 0.274 |
| Bingöl, Bitlis, Erzincan, Hakkari, Malatya, Muş | TSDC-2007 | 0.182 | 0.233 | 0.405 |
| Ağrı, Ardahan, Elazığ, Erzurum, Iğdır, Kars, Tunceli, Van | TSDC-2007 | 0.136 | 0.175 | 0.303 |

The fundamental natural period could be obtained by using eigenvalue analysis [95,96]. Based on the eigenvalue analysis, the natural periods were obtained as 0.55 s for the sample RC building. The same natural fundamental periods were obtained for all earthquake ground motion levels. The base shear forces for the sample structural model for each earthquake ground motion level were calculated. The comparison of the limit states of performance assessment for different earthquake ground motion levels is demonstrated in Figure 15. Table 12 lists all values obtained in the X direction.

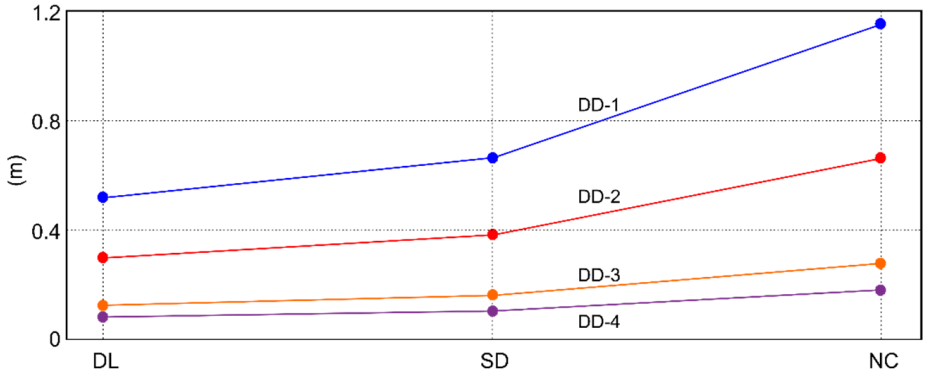


**Figure 15.** Comparison of limit states.

**Table 12.** Comparison of values obtained in the X direction for the sample building model for Bingöl.

| Earthquake Ground Motion Level | Base Shear | Displacement | K_elas | K-eff | DL | SD | NC |
|---|---|---|---|---|---|---|---|
| | (kN) | (m) | (kN)/m | (kN/m) | (m) | (m) | (m) |
| DD-1 | 9197.2 | 0.1194<br>0.2438<br>1.152 | 162,100.6 | 77,045.55 | 0.518 | 0.664 | 1.152 |
| DD-2 | 9193.25 | 0.119<br>0.2436<br>0.6624 | 162,100.6 | 77,224.23 | 0.298 | 0.382 | 0.662 |
| DD-3 | 9183.68 | 0.1191<br>0.2519<br>0.4229 | 162,100.6 | 77,325.8 | 0.125 | 0.161 | 0.278 |
| DD-4 | 9174.91 | 0.1187<br>0.2554<br>0.4221 | 162,100.6 | 77,078.87 | 0.082 | 0.104 | 0.181 |

Since the structural characteristics were the same, the base shear force, elastic, and effective stiffness values were approximately equal to each other. The larger values of the design spectra significantly increased the demand displacements expected from the building. The increase in the PGA for each ground motion level was approximately equal to the increase in the displacement values obtained for the performance levels. The displacement values expected from the building increased depending on the magnitude of the earthquake.

## 6. Conclusions

For assessing structural earthquake damage, developments in civil and earthquake engineering technologies require continuous updating of seismic design codes and seismic hazard maps. Both the codes and the seismic hazard maps were updated in 2018 in Turkey. In this study, some innovations were examined in detail within the scope of the last two codes, and comparisons were made. The Eastren Anatolian Region, which includes 14 provinces, is an excellent example due to its characteristics, such as its high seismicity, especially with the latest signficant earthquakes (2011 Van and 2020 Elazığ (Sivrice)). The region also experienced the 1939 Erzincan earthquake, which is the largest recorded earthquake in Turkey. In this respect, this region is in a position worth examining in terms of seismicity. It is well known that the seismic activity in Eastern Anatolia (Turkey) is very high. Both the historical and instrumental period earthquake presence listed here also show the high activity. Thus, it is of a great importance to perform seismic hazard estimation for the region. The findings showed that the highest Mo distribution was concentrated between the Van and Hakkari provinces. The fact that the recurrence periods of large earthquakes were proportional to the energy they accumulate can be explained by the high released

energy. Seismic hazard analyses were carried out using the updated earthquake hazard map of Turkey considering all the provincial centers in the Eastern Anatolian Region. The PGA and PGV values calculated for different probabilities of exceedance showed that the Bingöl province had the highest earthquake generation potential, while the Kars province had the lowest potential.

In the 2007 seismic code, in order to show the earthquake-prone areas, the country was divided into subregions. The provinces of Bingöl, Bitlis, Erzincan, Hakkari, Malatya, and Muş were classed as the first-degree earthquake hazardous region, which had the highest risk in terms of earthquake occurrence, while the other provinces were classified as the second-degree region. The most effective ground acceleration coefficient for the first-degree region was 0.40 g, while it was 0.30 g for the second-degree region. However, higher values were obtained via the updated code. The PGA values were calculated as 0.38–1.14 g for the probability of exceedance of 2%; 0.19–0.65 g for the 10% probability of exceedance; 0.07–0.28 g for the 50% probability of exceedance; and 0.05–0.18 g for the 68% probability of exceedance in 50 years for the provincial centers, according to the updated seismic hazard map. These discrepancies were caused by seismicity elements specific to the locations, the characteristics of fault or fault group, the distance from the fault or fault groups, and the earthquake history of the region, which are used in the updated code. Additionally, it is worth mentioning that calculation of the earthquake building parameters with site-specific analyses is the most important benefit of the updated code. Therefore, the behaviors of structures under an earthquake's effects can be obtained more accurately.

Even in the same earthquake zone and same ground conditions, differences between the current and previous methods were obtained for the spectral acceleration coefficients. The design spectral acceleration coefficient ($S_{DS}$) for the ZA local soil type was lower than the previous code for the Ağrı, Ardahan, Bitlis, Elazığ, Hakkari, Iğdır, Kars, Malatya, Muş, Tunceli, and Van provinces. Higher values were found for the Bingöl, Erzincan, and Erzurum provinces than the previous one. In the ZE local soil class type, while lower values were obtained in the Hakkari and Bitlis provinces, higher values were obtained for other provinces. The percentages of change between TSDC-2007 and TBEC-2018 in the design spectral acceleration coefficient ($S_{DS}$) were 29% in Bingöl for the ZE local soil type for the short period and 50% for Erzurum. While the spectral acceleration values in the previous code were the same for all soil classes in the same earthquake zones, they had different values for each local soil class and each geographical location with the current seismic design code. The current code takes into account both the local ground conditions and site-specific seismicity parameters. This reveals the importance of site-specific earthquake parameters.

Structural analyses were performed using the same design spectrum curve for Bingöl, Bitlis, Erzincan, Hakkari, Malatya, and Muş, which are in the first-degree earthquake hazard zone, and Ağrı, Ardahan, Elazığ, Erzurum, Iğdır, Kars, Tunceli, and Van, which are in the second-degree earthquake hazard zone in the previous hazard map. Therefore, the obtained values took on the same values for these provinces in the same earthquake hazard zone. Different results were obtained for all provinces in the region in the updated code and seismic hazard map. The necessity of site-specific seismicity calculations emerged once again. The target displacements were lower than the values predicted in TSDC-2007 for the Bitlis, Hakkari, Malatya, Muş, Ağrı, Ardahan, Iğdır, Kars and Van provinces. The values obtained for Bingöl, Erzincan, Elazığ, Erzurum, and Tunceli were higher than the values of TSDC-2007. The same target displacements were obtained in the same earthquake hazard zone in the previous seismic hazard map. However, the values obtained through the updated code were different for all of these provinces. As the PGA value increased, the demands for target displacement expected from the structure also increased when the ground motion increased, and more significant displacement of the structure was expected.

Four different earthquake ground motion levels were taken into account with TBEC-2018, while only one earthquake ground motion level was taken into account in TSDC-2007. Bingöl, which had the highest PGA value in the region, was chosen as an example in order to reveal the effect of different earthquake ground motion levels on the building

performance. For DD-1, which is the largest earthquake motion level, the expected target displacement values from the structure took on the largest values. The target displacements decreased as the earthquake repetition period decreased. The percentage of change in the target displacement values from DD-1 to DD-2 for different earthquake ground motion levels for the Bingöl province were 74% in DL, 74% in SD, and 74% in NC.

**Author Contributions:** Conceptualization, E.I., Y.L.E. and E.H.; methodology, A.B., E.I., Y.L.E. and E.H.; software, E.H. and E.I.; validation, A.B., E.I., Y.L.E. and E.H.; formal analysis, E.H.; investigation, E.I. and A.B.; resources, A.B., E.I., Y.L.E. and E.H.; data curation, E.I. and Y.L.E.; writing—original draft preparation, E.H. and E.I.; writing—review and editing, E.H., E.I. and Y.L.E.; visualization, Y.L.E.; supervision, A.B. and E.I.; project administration, E.I.; funding acquisition, E.H. All authors have read and agreed to the published version of the manuscript.

**Funding:** This research received no external funding.

**Institutional Review Board Statement:** Not applicable.

**Informed Consent Statement:** Not applicable.

**Data Availability Statement:** Most data are included in the manuscript.

**Acknowledgments:** We acknowledge the support of the German Research Foundation (DFG) and the Bauhaus-Universität Weimar within the Open-Access Publishing Programme. We are grateful to the reviewers for their constructive comments.

**Conflicts of Interest:** The authors declare no conflict of interest.

## References

1. Cornell, C.A. Engineering seismic risk analysis. *Bull. Seismol. Soc. Am.* **1968**, *58*, 1583–1606. [CrossRef]
2. Giardini, D.; Grünthal, G.; Shedlock, K.M.; Zhang, P. The GSHAP global seismic hazard map. *Ann. Geophys.* **1999**, *42*, 1225–1230. [CrossRef]
3. Kayabali, K. Modeling of seismic hazard for Turkey using the recent neotectonic data. *Eng. Geol.* **2002**, *63*, 221–232. [CrossRef]
4. Moehle, J.; Deirlein, G.G. A framework methodology for performance-based earthquake engineering. In Proceedings of the 13th World Conference on Earthquake Engineering, Vancouver, BC, Canada, 1–6 August 2004.
5. McGuire, R.K. Probabilistic seismic hazard analysis: Early history. *Earthq. Eng. Struct. Dyn.* **2008**, *37*, 329–338. [CrossRef]
6. Ozmen, B.; Can, H. Deterministic seismic hazard assessment for Ankara, Turkey. *J. Fac. Eng. Archit. Gazi Univ.* **2016**, *31*, 9–18. [CrossRef]
7. Yakut, A. Preliminary seismic performance assessment procedure for existing RC buildings. *Eng. Struct.* **2004**, *26*, 1447–1461. [CrossRef]
8. Harirchian, E.; Lahmer, T. Improved rapid visual earthquake hazard safety evaluation of existing buildings using a type-2 fuzzy logic model. *Appl. Sci.* **2020**, *10*, 2375. [CrossRef]
9. Işık, E. Consistency of the rapid assessment method for reinforced concrete buildings. *Earthq. Struct.* **2016**, *11*, 873–885. [CrossRef]
10. Hadzima-Nyarko, M.; Pavic, G.; Lesic, M. Seismic vulnerability of older confined masonry buildings in Osijek, Croatia. *Earthq. Struct.* **2016**, *11*, 629–648. [CrossRef]
11. Işık, E.; Işık, M.F.; Bulbul, M.A. Web based evaluation of earthquake damages for reinforced concrete buildings. *Earthq. Struct.* **2017**, *13*, 387–396. [CrossRef]
12. Harirchian, E.; Lahmer, T.; Buddhiraju, S.; Mohammad, K.; Mosavi, A. Earthquake safety assessment of buildings through rapid visual screening. *Buildings* **2020**, *10*, 51. [CrossRef]
13. Özmen, B.; Pampal, S. The evolution of earthquake zoning maps in Turkey. In Proceedings of the 4th International Earthquake Engineering and Seismology Conference, Eskişehir, Turkey, 11–13 October 2017.
14. Işık, E. A comparative study on the structural performance of an RC building based on updated seismic design codes: Case of Turkey. *Challenge* **2021**, *7*, 123–134. [CrossRef]
15. Akkar, S.; Kale, Ö.; Yakut, A.; Ceken, U. Ground-motion characterization for the probabilistic seismic hazard assessment in Turkey. *Bull. Earthq. Eng.* **2018**, *16*, 3439–3463. [CrossRef]
16. Akkar, S.; Azak, T.; Çan, T.; Çeken, U.; Tümsa, M.D.; Duman, T.Y.; Kale, Ö. Evolution of seismic hazard maps in Turkey. *Bull. Earthq. Eng.* **2018**, *16*, 3197–3228. [CrossRef]
17. Buyuksarac, A.; Isik, E.; Harirchian, E. A case study for determination of seismic risk priorities in Van (Eastern Turkey). *Earthq. Struct.* **2021**, *20*, 445–455. [CrossRef]
18. Güler, K.; Celep, Z. On the general requirements for design of earthquake resistant buildings in the Turkish Building Seismic code of 2018. In *IOP Conference Series: Materials Science and Engineering*; IOP Publishing: Bristol, UK, 2020; Volume 737, p. 012015.

19. Michetti, A.M.; Esposito, E.; Guerrieri, L.; Porfido, S.; Serva, L.; Tatevossian, R.; Vittori, E.; Audemard, F.; Azuma, T.; Clague, J.; et al. Environmental seismic intensity scale-ESI 2007. *Mem. Descr. Carta Geol. D'Ital.* **2007**, *74*, 41.
20. Silva, P.G.; Rodríguez-Pascua, M.A.; Giner Robles, J.L.; Élez, J.; Pérez-López, R.; Davila, M. Catalogue of the geological effects of earthquakes in Spain based on the ESI-07 macroseismic scale: A new database for seismic hazard analysis. *Geosciences* **2019**, *9*, 334. [CrossRef]
21. Aydınoğlu, M.N. A response spectrum-based nonlinear assessment tool for practice: Incremental response spectrum analysis (IRSA). *ISET J. Earthq. Technol.* **2007**, *44*, 169–192.
22. Doran, B.; Akbaş, B.; Sayım, I.; Fahjan, Y.; Alacalı, S.N. Uzun periyotlu bir yapıda yapısal sağlık izlemesi ve deprem performansının belirlenmesi. In Proceedings of the Turkey Conference on Earthquake Engineering and Seismology, Ankara, Turkey, 11–14 October 2011.
23. Fajfar, P. Analysis in seismic provisions for buildings: Past, present and future. *Bull. Earthq. Eng.* **2018**, *16*, 2567–2608. [CrossRef]
24. Midorikawa, M.; Okawa, I.; Iiba, M.; Teshigawara, M. Performance-based seismic design code for buildings in Japan. *Earthq. Eng. Eng. Seismol.* **2003**, *4*, 15–25.
25. Grünthal, G.; Wahlström, R. Sensitivity of parameters for probabilistic seismic hazard analysis using a logic tree approach. *J. Earthq. Eng.* **2001**, *5*, 309–328. [CrossRef]
26. Serva, L.; Vittori, E.; Comerci, V.; Esposito, E.; Guerrieri, L.; Michetti, A.M.; Mohammadioun, B.; Mohammadioun, G.C.; Porfido, S.; Tatevossian, R.E. Earthquake hazard and the Environmental Seismic Intensity (ESI) scale. *Pure Appl. Geophys.* **2016**, *173*, 1479–1515. [CrossRef]
27. Yunatçı, A.A.; Çetin, K.O. Site specific seismic response and soil liquefaction triggering assessment integrated within probabilistic seismic hazard framework. In Proceedings of the 6th National Conference on Earthquake Engineering, Istanbul, Turkey, 6–20 October 2007.
28. Harman, E.; Küyük, H. Probabilistic seismic hazard analysis for the city of Sakarya. *SAU J. Sci.* **2016**, *20*, 23–31.
29. Işık, E.; Büyüksaraç, A.; Ekinci, Y.L.; Aydın, M.C.; Harirchian, E. The effect of site-specific design spectrum on earthquake-building parameters: A case study from the Marmara region (NW Turkey). *Appl. Sci.* **2020**, *10*, 7247. [CrossRef]
30. Işık, E.; Ekinci, Y.L.; Sayil, N.; Büyüksaraç, A.; Aydın, M.C. Time-dependent model for earthquake occurrence and effects of design spectra on structural performance: A case study from the North Anatolian Fault Zone, Turkey. *Turk. J. Earth Sci.* **2021**, *30*, 215–234. [CrossRef]
31. TBEC-2018. *Turkey Building Earthquake Code*; Disaster and Emergency Management Presidency of Turkey: Ankara, Turkey, 2018.
32. Turkish Earthquake Hazard Map Interactive Web Application. Available online: https://tdth.afad.gov.tr (accessed on 2 February 2020).
33. Sucuoğlu, H. New improvements in the 2019 Building Earthquake Code of Turkey. *Turk. J. Earthq. Res.* **2019**, *1*, 63–75.
34. Işık, E.; Harirchian, E.; Bilgin, H.; Jadhav, K. The effect of material strength and discontinuity in RC structures according to different site-specific design spectra. *Res. Eng. Struct. Mater.* **2021**, *7*, 413–430. [CrossRef]
35. Aksoylu, C.; Arslan, M.H. Comparative investigation of different earthquake load calculation methods for reinforced concrete buildings in the 2007 and 2019 codes. *Int. J. Eng. Res. Devel.* **2021**, *13*, 359–374. [CrossRef]
36. Keskin, E.; Bozdoğan, K.B. Evaluation of 2007 and 2018 Turkish earthquake code for the province of Kirklareli. *Kırklareli Univ. J. Eng. Sci.* **2018**, *4*, 74–90.
37. Koçer, M.; Nakipoğlu, A.; Öztürk, B.; Al-hagri, M.G.; Arslan, M.H. Comparison of TBSC 2018 and TSC 2007 through the values of seismic load related spectral acceleration. *Selçuk-Tek. Derg.* **2018**, *17*, 43–58.
38. Karaşin, İ.B.; Işık, E.; Demirci, A.; Aydın, M.C. The effect of site-specific design spectra for geographical location on reinforced-concrete structure performance. *DUJE* **2020**, *11*, 1319–1330. [CrossRef]
39. Adar, K.; Büyüksaraç, A.; Işık, E.; Ulu, A.E. Comparison of 2007 and 2018 seismic codes in the scope of structural analysis. *Eur. J. Sci. Technol.* **2021**, *25*, 306–317. [CrossRef]
40. Peker, F.U.; Işık, E. A study on the effect of local soil conditions in TBDY-2018 on earthquake behavior of steel structure. *BEU J. Sci.* **2021**, *10*, 1125–1139. [CrossRef]
41. Nemutlu, Ö.F.; Balun, B.; Benli, A.; Sari, A. Investigation of the change of acceleration spectra in Bingöl and Elazığ provinces according to 2007 and 2018 Turkish Earthquake Codes. *DUJE* **2020**, *11*, 1341–1356. [CrossRef]
42. Ulutaş, H. Comparison of TEC (2007) and TBEC (2018) earthquake codes in terms of section damage limits. *Eur. J. Sci. Technol.* **2019**, *17*, 351–359. [CrossRef]
43. Balun, B.; Nemutlu, O.F.; Benli, A.; Sari, A. Estimation of probabilistic hazard for Bingol province, Turkey. *Earthq. Struct.* **2020**, *18*, 223–231. [CrossRef]
44. Yalın, M.; Ulutaş, H. An evaluation on seismic performance of an existing school building according to the 2007 and 2018 Turkish Seismic Codes. *NOHU J. Eng. Sci.* **2021**, *10*, 648–661. [CrossRef]
45. Yiğitbaş, E.; Elmas, A.; Sefunç, A.; Özer, N. Major neotectonic features of eastern Marmara region, Turkey: Development of the Adapazari-Karasu corridor and its tectonic significance. *Geol. J.* **2004**, *39*, 179–198. [CrossRef]
46. Ekinci, Y.L.; Ertekin, C.; Yiğitbaş, E. On the effectiveness of directional derivative based filters on gravity anomalies for source edge approximation: Synthetic simulations and a case study from the Aegean Graben System (Western Anatolia, Turkey). *J. Geophys. Eng.* **2013**, *10*, 035005. [CrossRef]
47. Ekinci, Y.L.; Yiğitbaş, E. Geophysical approach to the igneous rocks in the Biga Peninsula (NW Turkey) based on airborne magnetic anomalies: Geological implications. *Geodin. Acta* **2012**, *25*, 267–285. [CrossRef]

48. Ekinci, Y.L.; Yiğitbaş, E. Interpretation of gravity anomalies to delineate some structural features of Biga and Gelibolu peninsulas, and their surroundings (north-west Turkey). *Geodin. Acta* **2015**, *27*, 300–319. [CrossRef]
49. CGIAR-CSI GeoPortal. SRTM 90 m Digital Elevation Data. 2012. Available online: http://srtm.csi.cgiar.org (accessed on 10 September 2021).
50. Ateş, A.; Bilim, F.; Büyüksaraç, A.; Aydemir, A.; Bektaş, Ö.; Aslan, Y. Crustal structure of Turkey from aeromagnetic, gravity and deep seismic reflection data. *Surv. Geophys.* **2012**, *33*, 869–885. [CrossRef]
51. Aydemir, A.; Ates, A.; Bilim, F.; Büyüksaraç, A.; Bektas, O. Evaluation of gravity and aeromagnetic anomalies for the deep structure and possibility of hydrocarbon potential of the region surrounding Lake Van, Eastern Anatolia, Turkey. *Surv. Geophys.* **2014**, *35*, 431–448. [CrossRef]
52. Barka, A.A.; Kadinsky-Cade, K. Strike-slip fault geometry in Turkey and its influence on earthquake activity. *Tectonics* **1988**, *7*, 663–684. [CrossRef]
53. Ambraseys, N.N.; Melville, C.P. *A History of Persian Earthquakes*; 2005, Paperback Edition; Cambridge University Press: Cambridge, UK, 1982; 219p.
54. Şaroğlu, F.; Güner, Y. Doğu Anadolu'nun jeomorfolojik gelişimine etki eden ögeler: Jeomorfoloji, tektonik, volkanizma ilişkileri. *TJK Bülteni* **1981**, *24*, 119–130.
55. Ambraseys, N.N. Reassessment of earthquakes, 1900–1999, in the Eastern Mediterranean and the Middle East. *Geophys. J. Int.* **2001**, *145*, 471–485. [CrossRef]
56. Çelebi, E.; Aktas, M.; Çağlar, N.; Özocak, A.; Kutanis, M.; Mert, N.; Özcan, Z. 23 October 2011 Turkey/Van–Ercis earthquake: Structural damages in the residential buildings. *Nat. Hazards* **2013**, *65*, 2287–2310. [CrossRef]
57. DEMP. 2020. Available online: https://deprem.afad.gov.tr/tarihseldepremler (accessed on 2 April 2020).
58. Utkucu, M.; Durmus, H.; Yalçin, H.; Budakoglu, E.; Isik, E. Coulomb static stress changes before and after the 23 October 2011 Van, Eastern Turkey, earthquake (Mw = 7.1): Implications for the earthquake hazard mitigation. *Nat. Hazard Earth Syst.* **2013**, *13*, 1889. [CrossRef]
59. Isik, E.; Aydin, M.C.; Buyuksarac, A. 24 January 2020 Sivrice (Elazığ) earthquake damages and determination of earthquake parameters in the region. *Earthq. Struct.* **2020**, *19*, 145–156. [CrossRef]
60. Ambraseys, N.; Zatopek, A. *The Varto-Üstükran (E. Anatolia) Earthquake of 19 August 1966, a Field Report*; Unesco: Paris, France, 1968; 68p.
61. Guidoboni, E.; Traina, G. A new catalogue of earthquakes in the historical Armenian area from antiquity to the 12th century. *Anal. Geofis.* **1995**, *38*, 112–147. [CrossRef]
62. Tan, O.; Tapirdamaz, M.C.; Yörük, A. The earthquake catalogues for Turkey. *Turk. J. Earth Sci.* **2008**, *17*, 405–418.
63. Utkucu, M. 23 October 2011 Van, Eastern Anatolia, earthquake (M w 7.1) and seismotectonics of Lake Van area. *J. Seismol.* **2013**, *17*, 783–805. [CrossRef]
64. KOERI. 2020. Available online: http://www.koeri.boun.edu.tr/sismo/2/deprem-bilgileri/buyuk-depremler/ (accessed on 2 April 2020).
65. Aki, K. *Generation and Propagation of G Waves from the Niigata Earthquake of 16 June 1964, 2, Estimation of Earthquake Moment, Released Energy, and Stress-Strain Drop from G Wave Spectrum*; Earthquake Research Institute, The University of Tokyo: Tokyo, Japan, 1966; pp. 73–88.
66. Das, R.; Sharma, M.L.; Wason, H.R.; Choudhury, D.; Gonzalez, G. A seismic moment magnitude scale. *Bull. Seismol. Soc. Am.* **2019**, *109*, 1542–1555. [CrossRef]
67. Bormann, P.; Giacomo, D.D. The moment magnitude Mw and the energy magnitude Me common roots and differences. *J. Seismol.* **2010**, *15*, 411–427. [CrossRef]
68. Kostrov, V.V. Seismic moment and energy of earthquakes, and seismic flow of rock. *Izv. Acad. Sri. USSR Phys. Solid Earth* **1974**, *1*, 2344.
69. Hanks, T.; Kanamori, H. A moment magnitude scale. *J. Geophys. Res.* **1979**, *84*, 2348–2350. [CrossRef]
70. Bazzurro, P.; Cornell, C.A. Seismic hazard analysis of nonlinear structures. I: Methodology. *J. Struct. Eng.* **1994**, *120*, 3320–3344. [CrossRef]
71. Işık, E.; Kutanis, M.; Bal, İ.E. Displacement of the buildings according to site-specific earthquake spectra. *Period. Polytech-Civ.* **2016**, *60*, 37–43. [CrossRef]
72. Işık, E.; Kutanis, M. Determination of local site-specific spectra using probabilistic seismic hazard analysis for Bitlis Province, Turkey. *Earth Sci. Res. J.* **2015**, *19*, 129–134. [CrossRef]
73. Kutanis, M.; Ulutaş, H.; Işık, E. PSHA of Van province for performance assessment using spectrally matched strong ground motion records. *J. Earth Sys. Sci.* **2018**, *127*, 99. [CrossRef]
74. Pitilakis, K.; Riga, E.; Anastasiadis, A. Design spectra and amplification factors for Eurocode 8. *Bull. Earthq. Eng.* **2012**, *10*, 1377–1400. [CrossRef]
75. Andreotti, G.; Calvi, G.M. Nonlinear soil effects on observed and simulated response spectra. *Earthq. Eng. Struct. Dyn.* **2021**, *50*, 3831–3854. [CrossRef]
76. Andreotti, G.; Famà, A.; Lai, C.G. Hazard-dependent soil factors for site-specific elastic acceleration response spectra of Italian and European seismic building codes. *Bull. Earthq. Eng.* **2018**, *16*, 5769–5800. [CrossRef]
77. Stewart, J.P.; Afshari, K.; Goulet, C.A. Non-ergodic site response in seismic hazard analysis. *Earthq. Spectra* **2017**, *33*, 1385–1414. [CrossRef]

78. Abrahamson, N.A.; Silva, W.J. Empirical response spectral attenuation relations for shallow crustal earthquakes. *Seismol. Res. Lett.* **1997**, *68*, 94–127. [CrossRef]
79. Boore, D.M.; Joyner, W.B.; Fumal, T.E. Equations for estimating horizontal response spectra and peak acceleration from Western North American earthquakes: A summary of recent work. *Seis. Res. Lett.* **1997**, *68*, 128–153. [CrossRef]
80. Campbell, K.W.; Bozorgnia, Y. Updated near-source ground-motion (attenuation) relations for the horizontal and vertical components of peak ground acceleration and acceleration response spectra. *Bull. Seismol. Soc. Am.* **2003**, *93*, 314–331. [CrossRef]
81. Graizer, V.; Kalkan, E. Ground motion attenuation model for peak horizontal acceleration from shallow crustal earthquakes. *Earthq. Spectra* **2007**, *23*, 585–613. [CrossRef]
82. Ambraseys, N.N.; Douglas, J.; Sarma, S.K.; Smit, P.M. Equations for the estimation of strong ground motions from shallow crustal earthquakes using data from Europe and the Middle East: Horizontal peak ground acceleration and spectral acceleration. *Bull. Earthq. Eng.* **2005**, *3*, 1–53. [CrossRef]
83. Idriss, I.M. An NGA Empirical model for estimating the horizontal spectral values generated by shallow crustal earthquakes. *Earthq. Spectra* **2008**, *24*, 217–242. [CrossRef]
84. Seismosoft. SeismoStruct 2018—A Computer Program for Static and Dynamic Nonlinear Analysis of Framed Structures. 2018. Available online: http://www.seismosoft.com (accessed on 20 May 2021).
85. Antoniou, S.; Pinho, R. Advantages and limitations of adaptive and non-adaptive force-based pushover procedures. *J. Earthq. Eng.* **2004**, *8*, 497–522. [CrossRef]
86. Antoniou, S.; Pinho, R. Development and verification of a displacement-based adaptive pushover procedure. *J. Earthq. Eng.* **2004**, *8*, 643–661. [CrossRef]
87. Kutanis, M. Statik itme analizi yöntemlerinin performanslarının değerlendirilmesi. In Proceedings of the Yapısal Onarım ve Güçlendirme Sempozyumu, YOGS2006 Bildiriler Kitabı, Denizli, Turkey, 7–8 August 2006; pp. 205–210.
88. Pinho, R.; Antoniou, S. A displacement-based adaptive pushover algorithm for assessment of vertically irregular frames. In Proceedings of the Fourth European Workshop on the Seismic Behaviour of Irregular and Complex Structures, Thessaloniki, Greece, 26–27 August 2005.
89. Elnashai, A.S. Advanced inelastic static (pushover) analysis for earthquake applications. *Struct. Eng. Mech.* **2001**, *12*, 51–70. [CrossRef]
90. Mander, J.B.; Priestley, M.J.N.; Park, R. Theoretical stress-strain model for confined concrete. *J. Struct. Eng.* **1998**, *114*, 1804–1825. [CrossRef]
91. Menegotto, M.; Pinto, P.E. Method of analysis for cyclically loaded RC plane frames including changes in geometry and non-elastic behavior of elements under combined normal force and bending. Symposium on the resistance and ultimate deformability of structures acted on by well-defined repeated loads. In Proceedings of the International Association for Bridge and Structural Engineering, Zurich, Switzerland, 2–5 September 1973; pp. 15–22.
92. Antoniou, S.; Pinho, R. *Seismostruct–Seismic Analysis Program by Seismosoft*; Technical Manual and User Manual; Seismosoft: Pavia, Italy, 2003.
93. CEN. *Eurocode 8: Design of Structures for Earthquake Resistance—Part 3: Assessment and Retrofitting of Buildings*; EN 1998-3:2005; European Committee for Standardization: Brussels, Belgium, 2005.
94. Pinto, P.E.; Franchin, P. Eurocode 8-Part 3: Assessment and Retrofitting of Buildings. In Proceedings of the Eurocode 8 Background and Applications, Dissemination of Information for Training, Lisbon, Portugal, 10–11 February 2011.
95. Kutanis, M.; Boru, E.O.; Işık, E. Alternative instrumentation schemes for the structural identification of the reinforced concrete field test structure by ambient vibration measurements. *KSCE J. Civ. Eng.* **2017**, *21*, 1793–1801. [CrossRef]
96. Aksoylu, C.; Mobark, A.; Arslan, M.H.; Erkan, İ.H. A comparative study on ASCE 7-16, TBEC-2018 and TEC-2007 for reinforced concrete buildings. *Rev. Construcción* **2020**, *19*, 282–305. [CrossRef]